Environmental Science Nano

ROYAL SOCIETY OF CHEMISTRY

PAPER

View Article Online
View Journal | View Issue

Cite this: *Environ. Sci.: Nano*, 2024, **11**, 1296

Gold and titania nanoparticles accumulated in the body induce late toxic effects and alterations in transcriptional and miRNA landscape†

Andrea Soltysova, [ab] Nicole Ludwig, [c] Caroline Diener, [c] Monika Sramkova, [d] Katarina Kozics, [d] Kristina Jakic, [d] Lucia Balintova, [d] Neus Gomez Bastus, [e] Oscar Hernando Moriones, [e] Aurelia Liskova, [f] Zora Krivosikova, [g] Eva Rollerova, [h] Alena Manova, [i] Tibor Dubaj, [j] Victor Puntes, [e] Peter Simon, [j] Ladislava Wsolova, [h] Jana Tulinska, [f] Bozena Smolkova, ‡[k] Eckart Meese [c] and Alena Gabelova ‡*[d]

Received 19th December 2023,
Accepted 18th January 2024

DOI: 10.1039/d3en00954h

rsc.li/es-nano

The growing production of nanomaterials and their presence in consumer products raises fear about their impact on human health and the environment. Of particular concern are those nanomaterials that exhibit poor excretion and tend to accumulate in living organisms. Our study investigated the potential adverse biological effects of residual gold and titania nanoparticles (PEG-AuNPs and TiO_2NPs) 28 days after a single intravenous administration in rats. To comprehensively assess the potential health hazard of these metal nanoparticles (MNP), toxicological and transcriptomic analyses were employed. The liver was the primary organ of the MNP deposition, causing a reduction in the relative liver weight compared to unexposed animals. Concurrently, changes in serum biomarkers indicative of hepatic dysfunction and hematological and immunological alternations were determined. Integrated transcriptomic analysis unveiled exposure-induced effects on the rats' lungs, liver, and kidneys. The hepatic tissue, particularly in PEG-AuNPs-exposed rats, exhibited a noteworthy prevalence of deregulated genes, with functional classification spanning lipid metabolism, cell cycle, and cell proliferation pathways. Although the number of deregulated miRNAs was relatively modest compared to mRNA expression changes, both types of MNPs deregulated miR-203a, associated with liver injury, and miR-18a-5p and miR-32-5p linked to kidney damage. This study

Environmental significance

Metal nanoparticles (MNPs) are attractive nanostructured materials for many biomedical, industrial, and commercial applications, including cosmetics, food processing, and packing. Besides the apparent benefits, incomplete degradation and excretion after use raise concerns and uncertainties about their safety, which requires careful evaluation. In this work, we comprehensively investigate the biological effects of MNPs deposit in rat tissues for 28 days. The reduced relative liver weight and changes in serum biomarkers indicate variations in hepatic functions. Moreover, alterations determined in the transcriptional and miRNA expression landscape have been recently associated with liver injury and kidney damage. Our data emphasize the need for a more thorough assessment of the health effects of poorly soluble MNPs, deposited in the body due to their limited clearance. Integrating conventional toxicological and omics-based risk approaches contributes to a better understanding of the MNPs-triggered potential adverse effects.

[a] *Department of Molecular Biology, Faculty of Natural Sciences, Comenius University in Bratislava, 841 04 Bratislava, Slovakia*
[b] *Institute for Clinical and Translational Research, Biomedical Research Center, Slovak Academy of Sciences, 845 05 Bratislava, Slovakia*
[c] *Institute of Human Genetics, Saarland University, 66421 Homburg, Germany*
[d] *Department of Nanobiology, Cancer Research Institute, Biomedical Research Center, Slovak Academy of Sciences, 845 05 Bratislava, Slovakia.*
E-mail: alena.gabelova@savba.sk
[e] *Catalan Institute of Nanotechnology, UAB Campus, 08193 Bellaterra, Barcelona, Spain*
[f] *Institute of Immunology and Allergology, Slovak Medical University in Bratislava, 833 03 Bratislava, Slovakia*
[g] *Department of Clinical and Experimental Pharmacotherapy, Slovak Medical University in Bratislava, 833 03 Bratislava, Slovakia*
[h] *Department of Toxicology, Slovak Medical University in Bratislava, 833 03 Bratislava, Slovakia*
[i] *Institute of Analytical Chemistry, Slovak University of Technology in Bratislava, 812 37 Bratislava, Slovakia*
[j] *Institute of Physical Chemistry and Chemical Physics, Slovak University of Technology in Bratislava, 812 37 Bratislava, Slovakia*
[k] *Department of Molecular Oncology, Cancer Research Institute, Biomedical Research Center, Slovak Academy of Sciences, 845 05 Bratislava, Slovakia*

† Electronic supplementary information (ESI) available. See DOI: https://doi.org/10.1039/d3en00954h

‡ Equal contribution.

underscores the imperative for a more exhaustive biosafety assessment of poorly soluble MNPs that tend to deposit in the body. Such investigations are crucial for delineating the potential risks of these nanomaterials and guiding the development of adequate safety measures in their production and usage.

Introduction

Metal nanoparticles (MNPs), including metal oxide nanoparticles, such as gold, silver, titanium dioxide, or iron oxide nanoparticles, have become attractive nanostructured materials for a wide range of biomedical, commercial, and industrial applications. Their unique physicochemical properties (*e.g.*, optical, thermal, acoustic, magnetic, antibacterial, *etc.*), make them promising tools, especially in medicine, for more accurate imaging, diagnostics, and innovative therapeutic approaches.[1–3] MNPs are stable, easy to prepare, and functionalized by conjugation with antibodies, nucleic acids, and small molecules. Moreover, their intrinsic properties can be controlled by tuning their size and shape, providing multifunctional utility. For example, gold nanoparticles (AuNPs) have gained particular research interest due to their unique surface plasmon properties.[4] In medicine, they could be utilized as heating mediators/contrast agents in photothermal, photodynamic, and radiation therapy, X-ray imaging, or computed tomography.[5–7] The photosensitizing activity of titania nanoparticles (TiO_2NPs) found applications in photodynamic therapy, biosensors, nanocarriers for drug delivery, and antimicrobial agents.[8] In regenerative medicine, TiO_2 nanostructures are utilized as reinforcing materials and coating for the bare implant surfaces, providing hierarchical structures that enhance osteoblasts proliferation and differentiation and local delivery of osteoporosis drugs or antibiotics.[3] Moreover, AuNPs and TiO_2NPs are components of numerous consumer goods, especially in cosmetics and personal care products.[9,10] In the food industry, the distinctive attributes of MNPs offer significant advantages for food processing (as additives, preservatives, or carriers) and packing (mechanical, thermal, antibacterial, and barrier properties).[11,12] Candies, sweets, and chewing gum contain the highest TiO_2 content (more than 50% of TiO_2 particles are below 100 nm).[13]

After use, MNPs in foods, consumer products, or medications can enter the sewage treatment plants and end up in the environment as treated effluent discharged to surface waters or biosolids applied to agriculture as fertilizer. Knowledge about MNPs' concentration in the environment is currently insufficient. Based on the annual consumption of gold nanomaterials from medical applications, the average annual environmental concentration of AuNPs in sludge and surface water in the USA has been estimated at 45 μg kg^{-1} and 4.7 pg L^{-1}, respectively.[14] On the other hand, the median daily intake of food additive TiO_2 (E 171, 36% consisting of particles smaller than 100 nm) was estimated at 0.5–2 mg kg^{-1} body weight.[11,15] Particular concerns and uncertainties involve the persistence of MNPs in the organism due to negligible solubility and low excretion. Therefore, the biosafety of MNPs is particularly important and requires a thorough evaluation.[16–18]

Animal studies are a valuable tool to improve our knowledge of the fate of MNPs in the body and the host's response to exposure. Risk assessment studies most frequently investigate changes in histopathological, hematological, biochemical, and selected immune characteristics. Considering the amount of MNPs deposited in the body relative to the applied dose, conventional methods may overlook moderate MNP-mediated adverse effects. Therefore, objective assessment of their potential health hazard requires sophisticated and highly accurate approaches in addition to conventional techniques.[19,20] The advantage of omics technologies is their capacity to provide comprehensive information on exposure-induced molecular changes, allowing multidimensional profiling of complex biological systems. Moreover, omics technologies facilitate the discovery of predictive toxicity biomarkers, contributing to understanding biological mechanisms of action (MoA) or adverse outcome pathways (AOP).[21] In recent years, regulatory bodies such as ECHA (European Chemical Agency), EFSA (European Food Safety Authority), and OECD (Organisation for Economic Co-operation and Development) have strongly supported the development of new approach methodologies, integrating omics technologies into the hazard and risk assessment of new chemical substances and in particular of nanomaterials.[22]

Among omics technologies, transcriptomics plays a crucial role in enhancing our understanding of gene expression patterns. The transcriptome encompasses all the RNA transcripts, including coding (mRNA) and non-coding RNAs (miRNAs, lncRNAs, and circRNA), providing a comprehensive view of cellular RNA content. Their deregulation can have significant health consequences, given their vital role in governing critical cellular processes, such as proliferation, metabolism, apoptosis, morphogenesis, and differentiation.[23] Research focusing on long-term *in vivo* MNP exposure involving omics analysis is scarce. Toxicogenomics of mouse lung tissue was performed after exposure to TiO_2NPs,[24,25] and gene expression changes in the liver and spleen after intravenous administration of AuNPs were investigated in rats.[26] The vast majority of published data come from *in vitro* studies, mainly after short-term (24–72 h) exposure.[20,27] Integrating conventional toxicological approaches with omics analyses contribute to our comprehension of the MNPs-triggered adverse effects.

In our study, we investigated the systemic (hematological, biochemical, and immune) and local (histopathological) changes produced by residual PEGylated gold (PEG-AuNPs) and TiO_2NPs 28 days after single intravenous (iv) administration. In addition, we performed integrated transcriptomic analysis to elucidate exposure-induced mRNA

and miRNA expression dysregulation in lung, liver, and kidney tissues.

Materials and methods

Chemicals

Gold(III) chloride trihydrate ($HAuCl_4 \cdot 3H_2O$), trisodium citrate ($Na_3C_6H_5O_7$), tannic acid ($C_{76}H_{52}O_{46}$), potassium carbonate (K_2CO_3), polyethyleneglycol PEG-thiol, M_w 5000 (Ω-end = SH, α-end = OCH) were purchased from Thermo Fisher. Distilled water passed through a Millipore system (ρ = 18.2 MΩ) was used in all experiments. All glassware was rinsed with acetone and Millipore water before use.

Fabrication of gold and titanium dioxide nanoparticles

Synthesis of gold NPs. AuNPs were produced following Bastus *et al.*[28] In detail, a solution of 2.2 mM sodium citrate (SC) in Milli-Q water (150 mL) was heated with a heating mantle in a 250 mL three-necked round-bottomed flask for 15 min under vigorous stirring. A condenser was utilized to prevent the evaporation of the solvent. After boiling had commenced, 1 mL of $HAuCl_4$ (25 mM) was injected. The color of the solution changed from yellow to bluish-grey and then to soft pink and ruby-red in 10 min. The synthesized NPs are coated with negatively charged citrate ions and, hence, well suspended in H_2O. Later, the NPs were directly conjugated with a mercaptopolyethylene glycol monomethyl ether solution, having a final concentration of 2 μM of thiol-PEG stirring at 600 rpm for about 24 h. Finally, the conjugates were washed with pure water by centrifugation of 10.000*g* for 20 min and were concentrated five times to achieve a concentration of 0.396 mg Au per mL and ~4.05×10^{14} NPs per mL, respectively.

Synthesis of TiO_2NPs. Anatase NPs of ~5–10 nm have been synthesized based on a previously reported method.[29] Briefly, NaOH 3 M and HCl 3 M solutions were prepared. Afterward, 2.07 mL of titanium isopropoxide was added to the 10 mL acid solution. Once the solution was homogeneous, 30 mL of mQ water and 5 mL of the base solution were carefully added to the titania precursor solution; the pH was then adjusted to pH 5. The solution was left covered in an oven at 70 °C without stirring for 24 h. The resulting NPs were centrifuged twice, for the first time at 500*g* and the second time at 1000*g*, and resuspended in water. Afterward, they were thoroughly sonicated in a sonics bath for several hours, centrifuged at 1000*g*, and resuspended in 10 mM TMAOH.

Characterization of MNPs

UV-vis spectroscopy. UV-visible spectra were acquired with a Cary 60 spectrophotometer (Agilent). Measurements were performed using a quartz cuvette with a 10 mm light pathway at room temperature in the 200–800 nm range.

Dynamic light scattering and zeta potential. A Malvern ZetaSizer Ultra (Malvern Instruments, UK) operating at a light source wavelength of 532 nm and fixed scattering angle of 173° was used to measure NP hydrodynamic size and surface charge. The particle size and zeta potential were measured simultaneously three times. Previously to the characterization experiments, samples were purified to remove reactions by-products, excess, or surfactant. Measurements were conducted in a 1 cm path cell at 25 °C.

Transmission electron microscopy. The morphology of the NPs was visualized using FEI Magellan 400L XHR SEM in transmission mode operated at 20 kV. Morphology was also observed using a FEI Tecnai G2 F20 HR(S)TEM operated at 200 kV in Bright Field mode. A droplet (10 μL) of the sample after 5 min ultrasonication of a 1 : 5 dilution of the samples was drop cast onto a piece of the ultrathin carbon-coated 200-mesh copper grid (Ted-pella, Inc.) and left to dry in air. The samples' average size and size distribution were measured using Image Analysis software by counting at least 2000 particles.

The basic physicochemical characteristics of PEG-AuNPs and TiO_2NPs are presented in Table 1. No endotoxin contamination was found in PEG-AuNP and TiO_2NP solutions, with absorbance readings falling below detection levels (<0.005 EU mL^{-1}).

Experimental study design

Adult male Wistar rats (6–8 weeks old, average body weight 226 ± 7.4 g) were purchased from the Dobra Voda, Slovakia breeding farm. The animal study was approved by the Institutional Ethics Committee and the competent national authority (Registration no. Ro 2807/12-221). The experiment

Table 1 Basic physicochemical characteristics of the used MNPs

	PEG-AuNPs	TiO_2NPs
Core size [nm]	10.5 ± 0.83	5–10
Hydrodynamic size [nm]	13.0 ± 3.02	75.4 ± 6.96
Surface modification	PEG-thiol, M_w 5000 (Ω-end = SH, α-end = OCH)	—
PDI	0.2014 ± 0.019	0.258 ± 0.008
Concentration [NPs per mL] [mg mL^{-1}]	~4.05×10^{14}	~5×10^{15}
	0.396	5
Zeta-potential [mV]	−9.12 ± 1.58	−35.4 ± 0.61
Solvent	LPS-free sterile milli Q-water	TMAOH, 10 mM

Abbreviations: PDI – polydispersity index, PEG – polyethylene glycol, TMAOH – tetramethylammonium hydroxide.

was performed in the approved animal facility (license no. SK PC 14011), complying with Directive 2010/63/EU and Regulation 377/2012.

Rats were randomly divided into four experimental groups: i) control I group (n = 3) – phosphate-buffered saline (PBS, solvent for PEG-AuNPs), ii) control II group (n = 4) – tetramethylammonium hydroxide (TMAOH, solvent for TiO_2-NPs), iii) PEG-AuNPs group (n = 8), and iv) TiO_2NPs group (n = 8). Each animal was weighed before MNP administration, and individual MNP colloidal suspension volume was adjusted. A single dose of PEG-AuNPs (0.7 mg kg^{-1}) and TiO_2-NPs (7 mg kg^{-1}) was slowly injected into the rat tail vein. A detailed description of the MNP administration, animal sacrifice, and tissue sample collection was published recently.[30] The residual amount of MNPs that persisted in the blood, lungs, liver, spleen, and kidneys was assessed 28 days postinjection.

Quantification of MNPs in the organism

Residual PEG-AuNPs and TiO_2NPs were quantified by assessing elemental gold (Au) and titanium (Ti) content in selected tissues. The samples were mineralized using the microwave digestion system Multiwave GO (Anton Paar, Graz, Austria) using high-pressure Teflon vessels. The digestion of blood and tissues was carried out with a mixture of HNO_3–HCl (for Au) and HNO_3–H_2O_2 (for Ti), leading to complete mineralization. The microwave heating program was as follows: slow increase from room temperature to 170 °C for 20 min, hold for 10 min at 170 °C, and cooling for 10 min.

Graphite furnace atomic absorption spectrometry (GFAAS) equipped with a high-resolution atomic absorption spectrometer AA 700 (Analytic Jena, Jena, Germany) was used to quantify the internalized amount of Au. A standard 1.000 g L^{-1} gold solution was employed as a stock solution for AAS calibration; the detection limit was determined at 0.125 μg L^{-1}.

The internalized amount of Ti was determined by inductively coupled plasma mass spectrometry (ICP-MS) using the iCAP-Q ICP-MS instrument (Thermo Scientific, Bremen, Germany) operated in KED mode (helium CCT flow 5.00 mL min^{-1}). The sample ionization was performed at a plasma power of 1550 W using a PFA-ST nebulizer (argon flow 1.06 L min^{-1}; spray chamber temperature 2.70 °C). A stock standard solution of 1.000 g L^{-1} titanium was used for calibration; the limit of detection was determined as less than 0.100 μg L^{-1}.

Histopathology

The hematoxylin and eosin (H&E) staining was performed to visualize potential lung, liver, kidney, and spleen tissue lesions from control rats (injected with PBS and TMAOH) and MNP-administered animals. Tissue samples preserved in formalin were dehydrated and embedded in paraffin, and 4 μm-thick sections were prepared. The tissue structure of H&E stained individual organs was evaluated on a Motic (Hong Kong, China) light microscope equipped with a MOTICAM 3+ color CCD camera using the MOTIC IMAGES PLUS 3.0 ML (Hong Kong, China) software.

Hematological and biochemical analyses

After overnight fasting, the cardiac puncture for blood withdrawal was carried out while the animals were under anesthesia. Blood samples were collected using ethylenediamine tetra-acetic acid (EDTA) tubes. A hematological analyzer (Sysmex K-4500 (SYSMEX TOA Medical Electronics Co. LTD, Japan)) was used to determine: leukocyte count (WBC), erythrocyte count (RBC), hemoglobin (HGB), hematocrit (HCT), mean corpuscular volume (MCV), mean corpuscular hemoglobin (MCH), mean corpuscular hemoglobin concentration (MCHC), platelet count (PLT), percentage of lymphocytes (LYM %), and lymphocyte count (LYM).

Clinical chemistry was performed on an Ortho Clinical Vitros® 250 Chemistry System (Ortho-Clinical Diagnostics, Raritan, NJ, USA). Methodologies employed included colorimetric, potentiometric, and rate tests using multi-layered Vitros Slides. Evaluated serum parameters were: total protein (TP), albumin (ALB), urea (UREA), creatinine (CREAT), cholesterol (CHOL), triglycerides (TAG), aspartate aminotransferase (AST), alanine aminotransferase (ALT), calcium (Ca), magnesium (Mg), and phosphorus (P).

Determination of immune parameters

Phagocytic activity of granulocytes and monocytes and respiratory burst of phagocytes. The detailed procedure for the measurement of phagocytic activity and respiratory burst was published elsewhere.[31] In brief, 30 μL of rat heparinized whole blood was mixed with 10 μL of a working solution of dihydroethidium bromide (HE; Sigma-Aldrich, St. Louis, MO, USA) and incubated at 37 °C for 15 min. The HE working solution: 10 μL of HE stock solution (15.75 mg HE in 5 mL dimethylformamide; Merck, Kenilworth, NJ, USA) was added to 1 mL Medium 199 (Gibco, Invitrogen, Paisley, UK). Then, 3 μL of fluorescein-labeled *Staphylococcus aureus* bacteria (1.4×10^6 bacteria, Molecular Probes, Eugene, OR, USA) were put into each sample and incubated for another 15 min at 37 °C. Finally, 1 mL of cold lysis solution (0.829 g NH_4Cl, 0.1 g $KHCO_3$, and 0.0037 g Na_2EDTA dissolved in 100 mL water for injection) was added, and tubes were kept on ice for 10 min. Samples in duplicates were analyzed by a flow cytometer Cytomics FC 500 (Beckman Coulter) using forward and side scatter gates. The results were assessed by flow cytometry as follows: % of phagocytic granulocytes = phagocytic granulocytes/all granulocytes.

Mitogen-stimulated lymphocyte proliferation. Spleen cell suspension (2×10^6 cells per mL) in RPMI medium (Sigma-Aldrich, St. Louis, MO, USA) supplemented with 10% fetal calf serum (FCS, PAA, Linz, Austria) was dispensed in triplicate wells (150 μL per well) of a 96-well microtiter culture plate. Fifty microliters of particular mitogens were added to the individual wells and incubated for 48 h at 37

°C. The final concentrations of mitogens (Sigma-Aldrich, St. Louis, MO, USA) were as follows: concanavalin A (Con A; 2.5 μg mL^{-1}), phytohemagglutinin (PHA; 25 μg mL^{-1}), and pokeweed mitogen (PWM; 2.5 μg mL^{-1}). Each well was pulsed with 1 μCi [3*H*]-thymidine (Moravek Biochemicals, Brea, CA, USA) diluted in 20 μL medium for 24 h at 37 °C. Cells were harvested on glass filter paper, and radioactivity in the harvested materials (counts per minute) was measured using a Beta Scintillation counter Microbeta 2 (Perkin Elmer). Control splenocytes were cultured without mitogens (non-stimulated cultures).

Phenotypic analysis of spleen, lymph nodes, and thymus. The spleen, lymph nodes, and thymus were aseptically removed and placed in RPMI-1640 culture medium (Sigma-Aldrich, St. Louis, MO, USA), supplemented with 5 IU mL^{-1} heparin (Zentiva, Prague, Czech Republic) and 12 μg mL^{-1} gentamycin (Sandoz, Basel, Switzerland). The cell suspension was obtained by washing the organs with the culture medium in a syringe with a needle (spleen and thymus) or by homogenization with a piston (lymph nodes). Then, cells were centrifuged at 130*g* for 15 min and resuspended in an RPMI medium supplemented with 10% fetal calf serum (FCS, PAA, Linz, Austria) and standardized to the concentration of 2×10^6 cells per mL. Nine microliters of a mixture of labeled monoclonal antibodies were added to 90 μL of the spleen, lymph node, and thymus cell suspension and incubated in the dark for 30 min. Antibodies (eBioscience, San Diego, CA, USA) used to stain the cells were as follows: anti-rat CD3 FITC, anti-rat CD4 PE, anti-rat CD8a PerCP-eFluor 710, anti-rat CD45R PE, and anti-rat CD161 PerCP-eFluor 710. Isotype controls (mouse IgG3 Isotype Control-FITC, mouse IgG2a K Isotype Control-PE, mouse IgG1 K Isotype Control-PerCP-eFluor 710, and mouse IgG2b K Isotype Control-PE) were employed as negative controls to determine background fluorescence. Red blood cells were lysed with a lysis solution Versalyse (Beckman Coulter, CA, USA) for 15 min. Samples were analyzed using a flow cytometer Cytomics FC 500 (Beckman Coulter). The percentage of CD^{3+}, $CD^{3+}CD^{4+}$, CD^{3+}-CD^{8a+}, $CD^{3-}CD^{161+}$, and $CD^{3-}CD^{45R+}$ cells in each sample was measured in duplicates, using forward and side scatter gates.

Cytokine production by spleen cells. Splenocytes (2×10^6 cells per mL) were plated in triplicate wells (150 μL per well) on a 96-well plate and cultured with mitogens (Con A) at a final concentration of 2.5 μg mL^{-1} at 37 °C for 72 h. Then, the supernatants were collected and stored at −70 °C until analysis. The Cytokine & Chemokine 22-Plex Rat ProcartaPlex™ Panel (eBioscience) was used to measure the levels of interleukins (IL): IL-1α, IL-1β, IL-2, IL-4, IL-5, IL-6, IL-10, IL-12p70, IL-13, IL-17A, interferon-γ (IFN-γ), granulocyte-colony-stimulating factor (G-CSF), granulocyte-macrophage colony-stimulating factor (GM-CSF), tumor necrosis factor-α (TNF-α), macrophage inflammatory protein (MIP-1α, MIP-2), monocyte chemoattractant protein (MCP-1, MCP-3), interferon gamma-induced protein (IP-10), eosinophil chemotactic protein (eotaxin), chemokine (C-X-C motif) ligand 1 (CXCL1), and Rantes – regulated on activation, normal T cell expressed and secreted according to the manufacturer's instructions by an xMAP® equipment (Luminex, Madison, WI, USA).

RNA isolation

Three tissue samples from individual organs per group were used for microarray experiments. Eight tissues were collected for the validation experiments per each exposed group and three per each control group. Small tissue pieces (approx. 0.5 cm^3) were frozen in TRIzol® solution and stored at −80 °C until extraction. Total RNA was isolated using Direct-zol™ RNA Miniprep (Zymo Research, USA), and total RNA for miRNA expression analysis was isolated using miRNAeasy Mini Kit (Qiagen, Hilden, Germany) according to the manufacturer's instructions. RNA integrity number (RIN) was evaluated by capillary electrophoresis using Agilent RNA 6000 Nano Kit (Agilent Technologies, USA), and RNA quantity was measured using NanoDrop ND-2000 (Nanodrop Technologies, Inc., USA). Only RNA samples with RIN ≥ 8 were selected for transcriptome analysis, while samples with RIN above 7 were rated suitable for qPCR.

Gene expression microarray

The 100 ng of total RNA was labeled using the Low Input Quick Amp Labeling Kit (Agilent Technologies, USA) according to the manufacturer's instructions. Briefly, RNA was transcribed into cDNA using T7-primer and Affinity Script RNase Block Mix. All subsequent labeling reactions were performed using Cy3-dCTP for control samples and Cy5-dCTP for MNP samples to obtain labeled cRNA. Labeled cRNA was purified using GeneJET™ RNA Purification Kit (Thermo Fischer Scientific, USA) to remove non-incorporated nucleotides. The MNP sample was mixed with the appropriate control sample and fragmented (30 min incubation at 60 °C) using a Gene Expression Hybridization Kit (Agilent Technologies, USA). Samples were immediately applied onto SurePrint G3 Rat Gene Expression 8 × 60 K Microarray Slide (Agilent Technologies, USA) and hybridized for 17 h at 65 °C by rotating the slide at a speed of 10 rpm in Hybridization Oven (Agilent Technologies, USA). Afterward, hybridization, slides were washed (Gene Expression Wash Buffer Kit, Agilent Technologies, USA) and scanned at a resolution 2 μm using SureScan Microarray Scanner (Agilent Technologies, USA).

miRNA expression microarray

miRNA profiling was conducted using Agilent SurePrint Rat miRNA microarrays, release 21.0 in conjunction with miRNA Complete Labeling and Hybridization Kit according to manufacturer's instructions. In short, 100 ng total RNA was dephosphorylated and labeled using Cy3-dCTP. Labeled RNA was hybridized to the array slide for 20 hours at 55 °C and 20 rpm in the Agilent Hybridization oven. Afterward, slides were washed using the Gene Expression Wash buffers (Agilent Technologies, USA) and scanned in a SureScan Microarray

Scanner (Agilent Technologies, USA) at 3 μm resolution in double-pass mode.

Data analysis and *in silico* miRNA target prediction analyses

TIFF multiscan images from SureScan Microarray Scanner (Agilent Technologies, USA) were processed using Agilent Feature Extraction software. The raw data underwent quality control, normalization, and statistical analysis. Gene expression was analyzed using GeneSpring 14.9 GX software. A moderate *t*-test was applied to identify differentially expressed genes (DEGs). miRNA expression data were quantile normalized and analyzed using the R package. For each tissue, ANOVA analysis was performed to identify significantly deregulated miRNAs. In both analyses, p-value < 0.05 and fold change (FC) ≥ 1.5 were set as cut-offs. No miRNA and only a few mRNAs reached statistical significance after adjustment for multiple testing. It could be due to low-dose exposure and the small residual quantities determined in the organs, which might warrant important but mostly low changes in gene expression.

In silico miRNA target prediction analysis was done by implementing miRTargetlink 2.0,[32] miRDB,[33] and TargetScan[34] tools, in which rat species were selected to identify inversely correlated miRNA–mRNA pairs with potential predicted and validated interactions.

Validation of selected gene expressions using quantitative RT-PCR

For quantitative RT-PCR (qPCR), the total RNA was reverse transcribed using the RevertAid First Strand cDNA Synthesis Kit (Thermo Fisher Scientific, USA) according to the manufacturer's recommendations. The 20 μl qRT-PCR reaction contained 0.3 μM primers (Table S1†) and HOT FIREPol® EvaGreen® qPCR Mix Plus (Solis BioDyne, Estonia). Two pairs of housekeeping genes (*HPRT1* and *LDHA*) were selected to obtain more accurate results. qPCR was performed using Stratagene Mx3005P Real-time PCR System (Agilent Technologies, USA) with reaction conditions as follows: 95 °C for 10 min followed by 40 cycles of 95 °C for 30 s, 60 °C for 30 s, and 72 °C for 30 s. Gene expression changes were calculated by the $2^{-\Delta\Delta CT}$ method, and the results were averaged from triplicates for each sample (eight samples for each MNPs and three or four samples for PBS and TMAOH solvent controls, respectively).

Statistical analysis

The Shapiro–Wilk test was used to test for the normality of data distribution. Statistical comparisons between exposed and control groups were performed using the Mann–Whitney non-parametric test for unpaired samples. Data were presented as mean ± standard error of the mean (SEM). Statistical analysis was carried out using IBM SPSS software package version 23.0 (IBM SPSS, Inc., Chicago, IL, USA) and GraphPad Prism 6.01 (La Jolla, CA, USA). A p-value < 0.05 was considered statistically significant.

Results and discussion

Residual amounts of PEG-AuNPs and TiO_2NPs detected in selected animal organs

The determined quantities of Au and TiO_2 (the amount of Ti was converted to TiO_2) in the blood and selected organs 28 days after a single *iv* administration are shown in Table 2. The Au and TiO_2 amounts quantified in particular tissues were also expressed as a percentage of the initially injected dose to compare the efficacy of individual NP elimination from the organism.

Consistent with many other studies, the liver was the primary organ of MNP accumulation and persistence.[35,36] The total amount of residual Au determined in the liver (11.10 ± 1.15 μg) corresponded to approximately 7% of the applied dose (0.7 mg kg^{-1}), while for TiO_2 (0.47 ± 0.12 μg), it was less than 0.05%, although the injected dose was ten times higher (7 mg kg^{-1}). These results indicate much faster titania NP clearance from the organism compared to PEG-AuNPs. A key player in the pharmacokinetics, biodistribution, mechanisms of internalization, toxicity, and immune response of NPs is the biomolecular corona (BC), which spontaneously develops and evolves on the surface of nanomaterials immediately after they enter the body. BC composition is determined by the physicochemical properties of NPs (size, shape, and charge, but primarily by surface chemistry); it alters the nano-bio interface and endows NPs with a new biological identity. In nanomedicine, BC is believed to significantly contribute to the failure of promising nanodrugs in clinical trials.[37] PEGylation is the most commonly used surface modification of NPs for biomedical applications. It reduces the absorption of serum proteins on the surface of nanocarriers, thus prolonging the blood circulation time and preventing their rapid elimination by the reticuloendothelial system.[33] Differences in BC composition between PEG-AuNPs and bare titania NPs could significantly affect the accumulation and clearance rates of MNPs.

The fate of poorly degradable MNPs in the body has not yet been sufficiently investigated, and the potential biological hazard of deposit MNPs is a reason for concern. Despite low

Table 2 The residual amount of elemental gold (Au) and titanium dioxide (TiO_2) quantified in the blood and selected organs per gram of tissue determined by GFAAS in rats 28 days after a single *iv* injection

Sample	Au		TiO_2	
	[μg g^{-1}]	[%][a]	[μg g^{-1}]	[%][a]
Blood	0.05 ± 0.01	0.473	0.01 ± 0.002	0.015
Liver	2.15 ± 0.22	6.916	0.06 ± 0.01	0.017
Lungs	0.90 ± 0.16	0.613	0.03 ± 0.003	0.002
Kidneys	0.27 ± 0.10	0.221	0.03 ± 0.004	0.003
Spleen	4.42 ± 2.32	1.007	0.11 ± 0.02	0.003

[a] Residual amount of Au and TiO_2 in tissues expressed as a percentage of the initially applied dose. PEG-AuNPs (0.7 mg kg^{-1} = 100%), TiO_2NPs (7 mg kg^{-1} = 100%).

solubility, AuNPs, for example, have been shown to undergo intra-lysosomal biodegradation and self-assembly into biopersistent nanostructures.[38] Furthermore, low concentrations of particulate TiO_2 (0.01–0.16 mg kg^{-1}) have been identified in postmortem human liver samples, probably due to oral consumption.[39] The use of E171 in foodstuff is banned as it can no longer be considered safe.[40]

Health status and organ histology and relative organ weight

Residual MNPs did not cause any visible signs of morbidity in exposed animals. The rats showed normal physical activity without lethargy or apathy. While the increase in body weight (BW) of control rats in both control groups (PBS and TMAOH) was similar (28 and 26%, respectively), the BW of PEG-AuNPs-exposed animals increased only by 20.5%, and TiO_2NPs-injected rats by 21% (Fig. S1†). However, the difference in BW between controls and exposed rats was insignificant. On the other hand, a significantly lower relative liver weight (RLW, the liver weight/the body weight ratio) was detected in PEG-AuNPs-injected rats (Table 3). Although the RLW of TiO_2NPs-exposed animals was also lower than control rats, it did not reach significance. No differences in liver weights between controls and exposed animals were found seven days postinjection (data not shown). Differences in other relative organ weights between MNP-exposed rats and respective control animals were insignificant, although differences were noticeable, especially for PEG-AuNPs.

A complete microscopic examination of the organs (liver, lung, kidneys, and spleen) from controls (PBS and TMAOH) and MNP-exposed animals did not show gross pathological lesions in individual tissues 28 days after exposure. However, 24 hours after PEG-AuNP injection, cytoplasmic alteration and small vacuoles diffusely scattered through the whole hepatic tissue were observed. On day 7, visible hepatocyte vacuolation/cellular swelling was determined in the livers of both PEG-AuNP and TiO_2NP-exposed animals. The residual amounts of Au and Ti/TiO_2 determined in the liver at that time were 11.46 μg and 1.47 μg, respectively. Titania NPs induced milder cytoplasmic vacuolation (CV) than PEG-AuNPs, possibly due to the lower residual amount of TiO_2NPs determined in the liver (paper under preparation). Similar histological changes in rat hepatic tissue were reported by Abdelhalim *et al.*[41] and Yahyaei *et al.*[42] after exposure to bare AuNPs. Although CV, seen after a mild acute and subacute liver injury, should be reversible, it could also lead to cell death.[43] Cho *et al.*[44] reported liver damage, inflammation, and apoptosis in mice seven days after *iv* administration of 4.26 mg kg^{-1} of PEGylated gold NPs. As no histological changes were observed in the parenchymal liver tissue 28 days after exposure, it is plausible that the removal of damaged cells occurred through processes such as apoptosis/necrosis or other form of cell death. We could hypothesize that the reduced liver weight determined 28 days after MNP administration could result from removing damaged cells during liver regeneration. However, cellular stress responses/paracrine signals from injured epithelial cells may have affected intracellular signaling and epigenetic regulation.

Table 3 The liver, kidneys, spleen, and lungs weight of control and MNPs-exposed animals 28 days after exposure. Data are presented as means ± SEM. $^{**}p < 0.01$

Group	Liver [g]	Kidneys [g]	Spleen [g]	Lungs [g]
I	3.13 ± 0.14	1.05 ± 0.04	0.33 ± 0.03	0.93 ± 0.09
II	3.17 ± 0.26	1.09 ± 0.04	0.32 ± 0.01	0.82 ± 0.05
III	2.34 ± 0.12**	0.94 ± 0.02	0.28 ± 0.02	0.73 ± 0.03
IV	2.68 ± 0.13	1.15 ± 0.09	0.40 ± 0.05	0.78 ± 0.04

Abbreviation: group I – PBS, group II – TMAOH, group III – PEG-AuNPs, group IV – TiO_2NPs.

Biochemical and hematological analyses

No statistically significant differences between groups I and II were identified in biochemical, hematological, and immunological parameters (Table S2†). Therefore, data from both controls were pooled and used as one control for both exposed groups. The values for individual biochemical parameters analyzed in control and MNP-exposed rats are shown in Table S3.† In the PEG-AuNPs group, AST concentration was significantly elevated ($p < 0.01$), while ALT was reduced ($p < 0.05$) (Fig. 1). AST and ALT liver enzymes are valuable biomarkers of hepatocellular injury; however, an AST to ALT ratio (also termed De Ritis ratio) is considered a better predictor of liver function damage than individual enzymes. The clinical AST/ALT ratio limit for a chronic hepatic disease is ≥2.[45] The AST/ALT ratio of 2.9 determined in PEG-AuNPs-exposed rats might indicate changes in hepatic functions. At the same time, a significant increase in serum CHOL values ($p < 0.05$) was determined in both groups of MNP-injected rats. Although the TAG level detected in the serum of PEG-AuNPs-exposed rats was reduced ($p < 0.05$) compared to control animals, this value was within the reference range. Similarly, ALB and TP levels were elevated ($p < 0.05$) in the serum of MNP-exposed animals compared to controls; however, they were still within the normal range. In TiO_2NP-exposed rats, no significant differences in serum AST, ALT, and TAG values compared to control were identified (Fig. 1). Significant changes in several serum biochemical parameters identified in PEG-AuNPs-exposed animals indicate functional liver changes commonly associated with chronic liver disease.

Hematological profiling revealed a significant increase in red blood cells, hemoglobin, and hematocrit values in MNP-exposed rats (Table S4†). Detected polycythemia might be related to the interaction of residual MNPs with erythropoiesis. In addition, both MNPs raised the number of platelets and monocytes, but the values reached significance only in TiO_2NP-exposed animals. However, considering the values of historical controls, these changes were without significant toxicological relevance as they were within the reference range.[46]

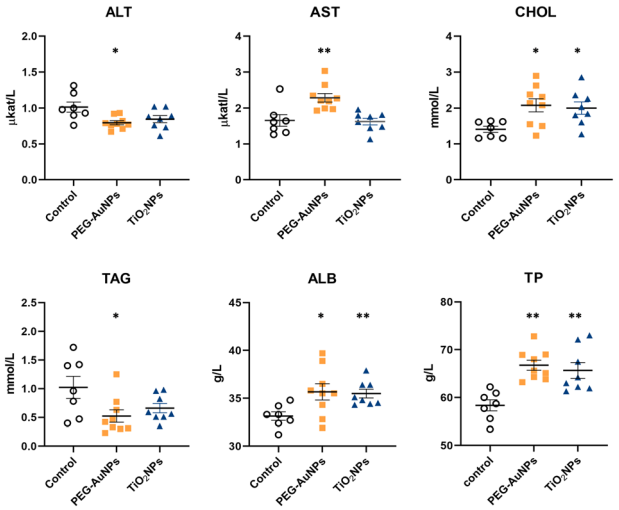

Fig. 1 Deregulation of selected biochemical parameters in MNP-exposed animals. ALT – alanine aminotransferase, AST – aspartate aminotransferase, CHOL – cholesterol, TAG – triglycerides, ALB – albumin, TP – total protein. Data are presented as mean ± SEM. *$p < 0.05$, **$p < 0.01$.

Immune response profiling

Phagocytosis, the first line of the cell-based defense system, is a vital biological activity protecting the host from internal and external threats and maintaining tissue homeostasis. No deviations in granulocyte phagocytosis and respiratory burst of leukocytes were observed in blood from MNP-injected animals compared to control rats. However, monocyte phagocytic activity was significantly suppressed in PEG-AuNPs-exposed animals but not in TiO_2NP-treated rats (Fig. S2A†).

Lymphocyte proliferation assay is frequently used to examine the functionality of cell-mediated immunity. A slight but insignificant reduction in Con A, PHA (T-cell-specific), and PWM (T-dependent B-cell-specific) stimulated responses were identified in splenic lymphocytes from PEG-AuNPs-injected rats compared to control animals (Fig. S2B†).

Phenotypic analysis of the spleen, lymph nodes, and thymus revealed a significant enhancement of $CD^{3-}CD^{45+}$ splenic lymphocytes (B-cells) in PEG-AuNPs-exposed animals and a significant suppression of $CD^{3+}CD^{8+}$ thymus cytotoxic T-cells in TiO_2NPs-exposed rats. All other evaluated parameters did not differ significantly from the controls (Table S5†).

The cytokine/chemokine secretion profile of mitogen-stimulated spleen cells from MNPs-exposed and control rats is shown in Table 4.

A significant decrease in several cytokines (IL-1β, IL-5, IL-6, IL-17A) and chemokines (MIP-2, MCP-1, MCP-3, eotaxin) was identified in spleen cell culture supernatants from PEG-AuNP-exposed rats. On the other hand, reduced production of IL-6 and GM-CSF ($p < 0.01$) was only found in TiO_2NP-exposed animals compared to the control.

Whole-genome transcriptional changes induced by residual MNPs

The whole-genome MNP exposure-induced expression changes were assessed in three organs, the lung, liver, and kidneys, 28

Table 4 Cytokine and chemokine levels in spleen cell culture supernatants determined 28 days after a single *iv* MNP administration

Cytokine/chemokine	Unit	Controls (n = 7)	PEG-AuNPs (n = 9)	TiO_2NPs (n = 8)
IL-1α	pg mL^{-1}	644.72 ± 54.62	546.11 ± 27.33	593.29 ± 36.50
IL-1β	pg mL^{-1}	68.07 ± 10.64	40.31 ± 5.79*	50.43 ± 8.06
IL-2	ng mL^{-1}	12.37 ± 0.68	11.24 ± 0.67	11.69 ± 0.73
IL-4	pg mL^{-1}	50.05 ± 13.73	32.13 ± 5.48	79.92 ± 27.64
IL-5	pg mL^{-1}	73.82 ± 16.89	28.11 ± 3.96*	52.47 ± 10.56
IL-6	pg mL^{-1}	18.35 ± 1.84	12.35 ± 1.32**	9.00 ± 1.00**
IL-10	ng mL^{-1}	5.28 ± 1.22	2.78 ± 0.40	5.15 ± 1.50
IL-12p/70	pg mL^{-1}	349.30 ± 31.97	288.70 ± 28.56	318.01 ± 34.85
IL-13	pg mL^{-1}	22.94 ± 4.70	15.37 ± 1.67	24.05 ± 5.38
IL-17A	pg mL^{-1}	543.48 ± 168.12	144.21 ± 18.00**	331.25 ± 94.17
IFN-γ	ng mL^{-1}	45.09 ± 7.93^{ac}	49.23 ± 5.99^{ac}	50.32 ± 6.68^{ac}
G-CSF	ng mL^{-1}	nd	nd	nd
GM-CSF	pg mL^{-1}	65.40 ± 7.79	57.69 ± 6.51	31.08 ± 4.63**
TNF-α	pg mL^{-1}	170.03 ± 25.50	111.38 ± 19.31	123.68 ± 25.15
MIP-2	pg mL^{-1}	151.64 ± 25.41	84.59 ± 10.83*	122.02 ± 16.88
MCP-1	ng mL^{-1}	51.64 ± 4.06	28.07 ± 2.51**	41.63 ± 5.65
MCP-3	ng mL^{-1}	2.35 ± 0.21	1.55 ± 0.16*	2.04 ± 0.23
IP-10	ng mL^{-1}	12.70 ± 0.87	11.80 ± 0.77	11.14 ± 0.67
Eotaxin	pg mL^{-1}	22.30 ± 1.56	17.22 ± 1.12*	20.46 ± 1.49
CXCL1	pg mL^{-1}	247.44 ± 11.52	237.16 ± 6.34	233.08 ± 6.32
Rantes	ng mL^{-1}	22.27 ± 5.67	16.36 ± 2.41	13.29 ± 1.99

Abbreviations: IL – interleukin, IFNγ – interferon-gamma, G-CSF – granulocyte-colony stimulating factor, GM-CSF – granulocyte-macrophage colony-stimulating factor, TNF-α – tumor necrosis factor-alpha, MIP-2 – macrophage inflammatory protein 2, MCP-1 – monocyte chemoattractant protein 1, MCP-3 – monocyte-chemotactic protein 3, IP-10 – interferon gamma-induced protein 10, eotaxin – eosinophil chemotactic protein, CXCL1 – chemokine (C-X-C motif) ligand 1, Rantes – regulated on activation, normal T cell expressed and secreted, nd – not detected, ac – above calibration curve.

Table 5 The number of deregulated entities/genes determined in lung, liver, and kidney 28 days after MNPs exposure with selected cut-offs $p < 0.05$ and fold change ≥ 1.5

Deregulated entities/genes	PEG-AuNPs			TiO_2NPs		
	Lung	Liver	Kidney	Lung	Liver	Kidney
Total	241/162	3429/2458	300/238	463/355	821/599	591/437
Up-regulated	207/136	1915/1325	226/176	127/72	434/372	274/226
Down-regulated	34/26	1514/1133	74/62	336/283	387/227	317/211

days after a single injection. These organs were selected because the liver and kidneys play an essential role in MNP elimination *via* the hepatobiliary route or renal clearance, depending on the particle size.[47] Also, the lungs are exposed to MNPs after *iv* application because deoxygenated blood primarily passes to the lungs. Microarray analysis revealed a large number of significantly deregulated entities/genes ($p < 0.05$) with FC cut-off ≥ 1.5 (Tables 5 and S6†). For both MNPs, the most abundant gene expression changes were identified in the liver, followed by the kidneys and lungs; however, the numbers of deregulated genes (DEGs) varied substantially between particular MNPs. Notably, the residual PEG-AuNPs deregulated a 4-fold higher number of genes than TiO_2NPs, which positively correlates with the residual MNP amounts quantified in this organ.

The physicochemical properties of NPs can significantly affect the gene expression pattern both *in vitro* and *in vivo*. Depending on their surface modifications, spherical AuNPs induced expression of distinct genes in the mouse liver 7 days after *iv* administration.[48] PEG-AuNP deregulated the fewest number of genes, while polyethyleneimine-capped (PEI)-AuNPs deregulated the most. Only 24 genes from 1720 deregulated genes (DEGs) overlapped among PEG-, chitosan (CS)-, and PEI-AuNPs. On the cotrary, Falagan-Lotsch *et al.*[49] reported that PEG-coated gold rods, compared to other surface coatings, elicited the most significant modifications in gene expression. Differences in gene expression profiles were observed *in vitro* following short-term exposure to AuNPs, depending on surface coating, cell types, and dosing.[50] Deregulation of gene expression patterns was detected in human bone marrow stromal cells with differently sized TiO_2NPs.[51] Smaller titania NPs induced genes associated with antivirus defense, while larger TiO_2NPs activated genes linked to proliferation and differentiation. Size-dependent changes in gene expression profiles were also

Table 6 List of 10 top deregulated genes determined 28 days after MNPs exposure in individual organs

	Probe name	*p*-value	FC	Gene symbol	Probe name	*p*-value	FC	Gene symbol
	PEG-AuNPs				TiO_2NPs			
Lungs	A_64_P133997	9.28×10^{-3}	6.80	*Gpr35*	A_42_P602724	3.44×10^{-3}	17.73	*Ubd*
	A_44_P1117889	9.18×10^{-3}	−6.15	*LOC103691118*	A_64_P112429	1.17×10^{-2}	−15.41	*Defb5*
	A_44_P1153189	3.68×10^{-3}	5.75	*LOC683422*	A_64_P072983	4.14×10^{-4}	13.06	*RGD1562136*
	A_44_P1085641	4.50×10^{-2}	−5.47	*Cox6a2*	A_42_P548410	9.40×10^{-3}	10.64	*Acot1*
	A_44_P1084096	3.97×10^{-3}	5.06	*Acot1*	A_64_P098501	1.80×10^{-3}	10.43	*Tubb1*
	A_64_P085530	2.08×10^{-3}	−4.45	*Scd*	A_43_P15362	1.66×10^{-2}	−10.19	*Slc9a5*
	A_44_P1102793	2.26×10^{-3}	4.41	*Dchs2*	A_64_P081352	2.38×10^{-2}	−8.86	*Kcnc3*
	A_64_P088382	4.48×10^{-2}	4.11	*Angptl4*	A_64_P112185	3.04×10^{-2}	−8.62	*Nebulin*
	A_42_P736573	1.80×10^{-2}	4.03	*Pdk4*	A_64_P010268	4.51×10^{-3}	−8.19	*LOC102556662*
	A_44_P1156522	5.78×10^{-3}	3.82	*Ttc24*	A_44_P111662	1.07×10^{-2}	−8.17	*Ly49s3*
Liver	A_64_P085530	5.72×10^{-4}	−103.52	*Scd*	A_44_P552452	1.27×10^{-6}	64.62	*RT1-Bb*
	A_43_P12619	8.06×10^{-6}	63.81	*Nr4a3*	A_64_P146165	3.00×10^{-2}	−23.23	*RGD1560242*
	A_42_P836392	2.25×10^{-3}	−56.70	*Elovl6*	A_64_P091935	7.08×10^{-5}	−14.61	*Scd4*
	A_64_P111315	2.43×10^{-4}	−55.07	*Ropn1l*	A_64_P085530	5.66×10^{-4}	−12.40	*Scd*
	A_44_P428691	1.49×10^{-3}	−49.33	*Elovl6*	A_64_P154537	1.42×10^{-3}	−12.09	*LOC681458*
	A_44_P654444	5.51×10^{-6}	41.07	*Nr4a3*	A_43_P13004	2.29×10^{-2}	11.37	*Cdh17*
	A_44_P1127297	2.29×10^{-5}	38.75	*LOC103692696*	A_42_P836392	3.56×10^{-3}	−10.41	*Elovl6*
	A_64_P091935	6.07×10^{-4}	−38.40	*Scd4*	A_42_P585995	5.30×10^{-3}	10.03	*Nim1k*
	A_44_P1135742	1.62×10^{-2}	−37.28	*LOC102547310*	A_64_P095005	8.88×10^{-6}	9.31	*Mmd2*
	A_44_P235978	5.02×10^{-5}	−36.97	*Fasn*	A_64_P097425	2.65×10^{-4}	9.05	*LOC683761*
Kidneys	A_44_P1017367	3.53×10^{-2}	375.41	*Alb*	A_64_P058829	5.27×10^{-6}	24.46	*LOC685081*
	A_43_P12402	2.30×10^{-2}	293.80	*Slc27a5*	A_64_P098501	3.22×10^{-5}	21.64	*Tubb1*
	A_44_P1143828	3.22×10^{-2}	−51.04	*LOC102553583*	A_44_P524748	6.86×10^{-5}	17.88	*Olr1076*
	A_44_P128147	4.74×10^{-2}	40.93	*Tf*	A_64_P064336	5.75×10^{-4}	15.26	*RT1-T18*
	A_44_P473510	1.84×10^{-3}	35.25	*Vsig4*	A_64_P100023	9.73×10^{-4}	14.13	*Zcchc3*
	A_64_P132721	2.38×10^{-2}	−24.83	*Oacyl*	A_42_P684885	1.88×10^{-3}	10.67	*Atp12a*
	A_64_P058087	2.70×10^{-2}	24.45	*Rbp4*	A_64_P072983	4.72×10^{-4}	9.69	*Macir*
	A_64_P157371	3.72×10^{-2}	−17.75	*Pdpn*	A_64_P056583	6.75×10^{-4}	9.51	*Rhbdl3*
	A_44_P947608	1.28×10^{-2}	17.47	*Corin*	A_64_P014096	4.18×10^{-4}	8.51	*Htr3a*
	A_64_P072103	2.13×10^{-2}	−16.00	*Hmx2*	A_64_P072189	1.23×10^{-3}	7.13	*Mgat3*

determined in mouse lungs 28 days after the instillation of titanium dioxide NPs.[52]

The top ten deregulated genes in individual organs due to long-term MNP exposure are listed in Table 6. The FCs ranged between 375.4 and −103.5 for PEG-AuNPs and 64.6 and −23.2 for TiO_2NPs.

Gene expression changes were organ-specific (Fig. 2A and B). No common deregulated gene was identified in all organs analyzed from animals injected with PEG-AuNPs. In contrast, three common up-regulated genes *Tubb1* (*tubulin*, *beta 1 class VI*), *RT1-T18* (*RT1 class Ib*, *locus T18*), and *Rhbdl3* (*rhomboid like 3*) were identified in all three organs of TiO_2NPs-exposed rats. Conversely, both MNPs consistently deregulated a limited number of genes in the lungs (n = 4) (Fig. 2C, Table S6†). Notably, *Acot1* (*acyl-coenzyme A thioesterase 1*) and *Rhbdl3* (*rhomboid-like 3*) exhibited up-regulation, while *Scd* (*stearoyl-CoA desaturase*), and *Vom2r72* (*vomeronasal2 receptor 72*) were down-regulated.

The number of commonly deregulated genes was relatively high in the liver (n = 244) (Fig. 2D, Table S7†). The 10 top-down-regulated genes were mainly involved in fatty acid biosynthesis and metabolism. To this group belong *Scd* (*stearoyl-coenzyme A desaturase*), *Elovl6* (*elongation of long-chain fatty acid family member 6*), *Scd4* (*stearoyl-coenzyme A desaturase 4*), *Fasn* (*fatty acid synthase*), and *Fabp5* (*fatty acid binding protein 5*). From others, it was *Cxcl1* (*C-X-C motif chemokine ligand 1*), *Rrm2* (*ribonucleotide reductase regulatory subunit M2*), and *LOC681458* (*similar to stearoyl-coenzyme A desaturase 3*). *Nim1k* (*NIM1 serine/threonine protein kinase*) and *Rab30* (*RAB30*, member RAS oncogene family) were among the top up-regulated genes. *Scd*, *Scd4*, and *Elovl6* encode proteins playing a rate-limiting role in fatty acid biosynthesis. In the animal study performed by Piccinin *et al.*, Scd suppression resulted in an imbalance between saturated and monounsaturated fatty acids, a decrease in *de novo* lipogenesis, and an increase in β-oxidation of fatty acids. In addition, the animals displayed liver injury and fibrosis.[53] The ratio of saturated/monounsaturated affects cell growth and differentiation regulation, and its alteration has been implicated in various diseases, including liver dysfunction. Furthermore, decreased ELOVL6 expression level serves as a biomarker for poor prognosis in hepatocellular carcinoma.[54]

In general, lipid metabolism is closely linked to cell division because phospholipids constitute essential components of cytoplasmic membranes. Inhibition of fatty acid synthesis has demonstrated the ability to induce cell cycle arrest by preventing the exit from mitosis.[55]

Hepatocyte self-renewing is a critical step in liver regeneration. Ow *et al.*[56] have recently reported an association between lipid metabolism disorder and defects in hepatocyte proliferation in liver diseases. They showed that losing CDK1 (cyclin-dependent kinase 1) activity in hepatocytes could contribute to hepatic pathology. Interestingly, four genes functioning in the cell cycle and cell proliferation regulation (*Cdk1*, *Cdca3*, *Knstrn*, and *Spc25*) were down-regulated in the hepatic tissues of MNPs-exposed animals. In addition to Cdk1, inhibition of the cell division cycle associated 3 protein encoded

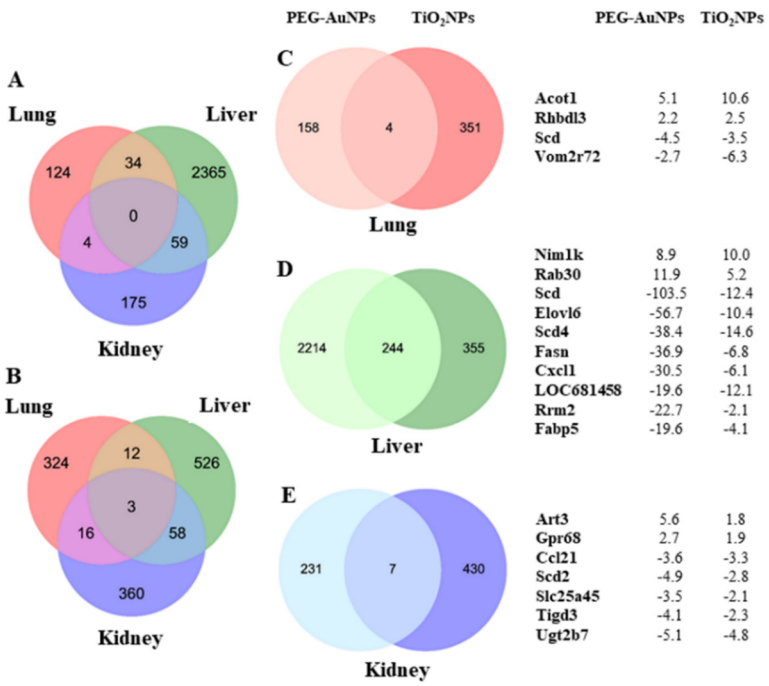

Fig. 2 Venn diagrams showing the number of deregulated genes overlapping between analyzed organs after PEG-AuNPs (A) and TiO_2NPs (B) exposure. The overlapping genes between studied MNPs in individual organs deregulated in the same direction by both studied MNPs are presented in the middle panel, C – lung, D – liver, and E – kidney. The right panel provides an overview of overlapping genes with fold change; only the top 10 overlapping genes are listed for the liver.

by *Cdca3* causes a block of cell proliferation and senescence.[57] Similarly, the kinetochore-localized astrin/SPAG5-binding protein encoded by *Knstrn* and Spindle pole body component 25 homolog encoded by *Spc25* are mitosis-associated spindle components promoting chromosome segregation during mitosis. Their suppression is associated with inhibition of proliferation and invasion.[58] Although *MafB*, (*bZIP Transcription Factor B*) acts as an oncogene in hepatocellular carcinoma and its upregulation is associated with disease progression,[59] *MafB* may also play a role in tissue repair as a regulator of tissue-resident macrophages that restrain the immune system and maintain homeostasis.[60] *Rab30*, a member of the RAS oncogene superfamily, encodes the protein with GTPase activity and is involved in the structural maintenance of the Golgi apparatus. Its up-regulation was identified in liver regeneration.[61] Up-regulation of both *MafB* and *Rab30* expression detected in MNPs-exposed rats might indicate an adaptive mechanism of the exposed tissue against the long-term presence of residual MNPs.

Interestingly, both MNPs up-regulated *Slc38A2* (*glutamine transporter Slc38A2*) and *Wsb1* (*WD Repeat and SOCS Box Containing 1*) genes, whose function is closely related to liver fibrosis and tumorigenesis. *Slc38A2* overexpression triggers a cancer-like metabolic profile as glutamine is known to be the exchanger for many essential amino acids in abnormal dividing cells, including cancer cells.[62] Wsb1 protein is supposed to be involved in regulating the epithelial–mesenchymal transition (EMT) process[63] and correlated with tumor progression, metastasis, and drug resistance.[64]

The residual PEG-AuNPs deregulated almost 10 times fewer genes in the kidneys than in liver tissue. However, the number of alterations in gene expression in renal and hepatic tissues was comparable in TiO_2NP-exposed rats. Strikingly, TiO_2NPs deregulated nearly 2-fold more genes in renal tissue than PEG-AuNPs despite much less residual TiO_2 being determined in renal tissue. In contrast to the liver, only a few common genes were found (n = 7) (Fig. 2E, Table S6†). Commonly up-regulated genes by both MNPs were *Art3* (*ADP-ribosyltransferase 3*) and *Gpr68* (*G protein-coupled receptor 68*). Down-regulated genes were *Ccl21* (*Chemokine (C-C motif) ligand 21*), *Scd2* (*Stearoyl-CoA desaturase 2*), *Slc25a45* (*Solute carrier family 25 member 45*), *Tigd3* (*Tigger Transposable*

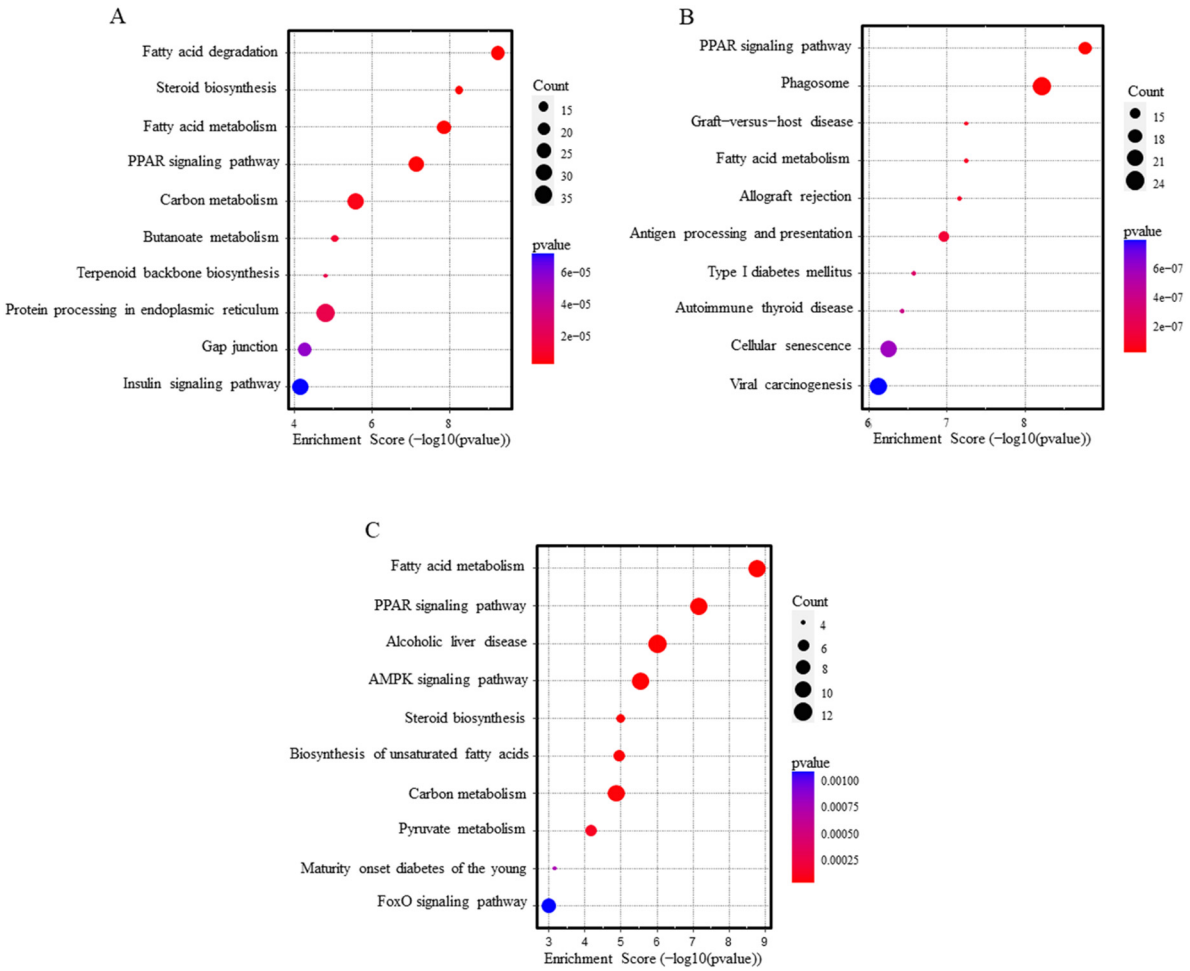

Fig. 3 Pathway analysis dot blots show the top 10 KEGG pathways enriched in the liver after PEG-AuNPs (A), TiO_2NPs (B) exposure, and overlapping genes (C).

Table 7 The number of deregulated miRNAs determined in lung, liver, and kidney 28 days after MNP exposure with selected cut-off criteria $p < 0.05$ and FC ≥ 1.5

Deregulated	PEG-AuNPs			TiO_2NPs		
miRNA	Lung	Liver	Kidney	Lung	Liver	Kidney
Total	2	2	14	6	16	22
Up-regulated	1	1	7	5	12	12
Down-regulated	1	1	7	1	4	10

Element-Derived Protein 3), and *Ugt2b7* (*UDP Glucuronosyltransferase Family 2 Member B7*). *ART3* is involved in cell cycle progression, cell differentiation, DNA repair, and regulation of inflammatory responses.[65] Its upregulation may be directly related to the defense of renal cells against the MNP deposit. GPR68 is a proton-sensing receptor involved in pH homeostasis and regulates various cellular functions. GPR68 up-regulation, detected in numerous cancer types, can help cells respond to extracellular acidosis.[66] UGT2B7, one of the Ugt enzymes, plays a central role in renal clearance. Interestingly, Margaillan *et al.*[67] found a significantly decreased glucuronidation capacity of neoplastic kidneys compared to normal kidneys, which correlated with substantially reduced UGT2B7 mRNA and protein expression.

Twelve genes, namely *Cdca3*, *Cdk1*, *Cxcl1*, *Knstrn*, *Spc25*, *Mafb*, *Nim1k*, *Nr4a2*, *Rab30*, *Spice1*, *Slc38a2*, and *Wsb1*, were selected for validation by qRT-PCR to confirm the relevance of the microarray data. Since the liver was the primary organ of MNPs accumulation and gene expression deregulation, these genes were selected using the following criteria: top-ranked genes deregulated in the same direction by PEG-AuNPs and TiO_2NPs, not involved in fatty acid metabolism. The validation experiments used a larger sample size and relevant controls for particular MNPs ($n = 3$ – PBS, $n = 8$ PEG-

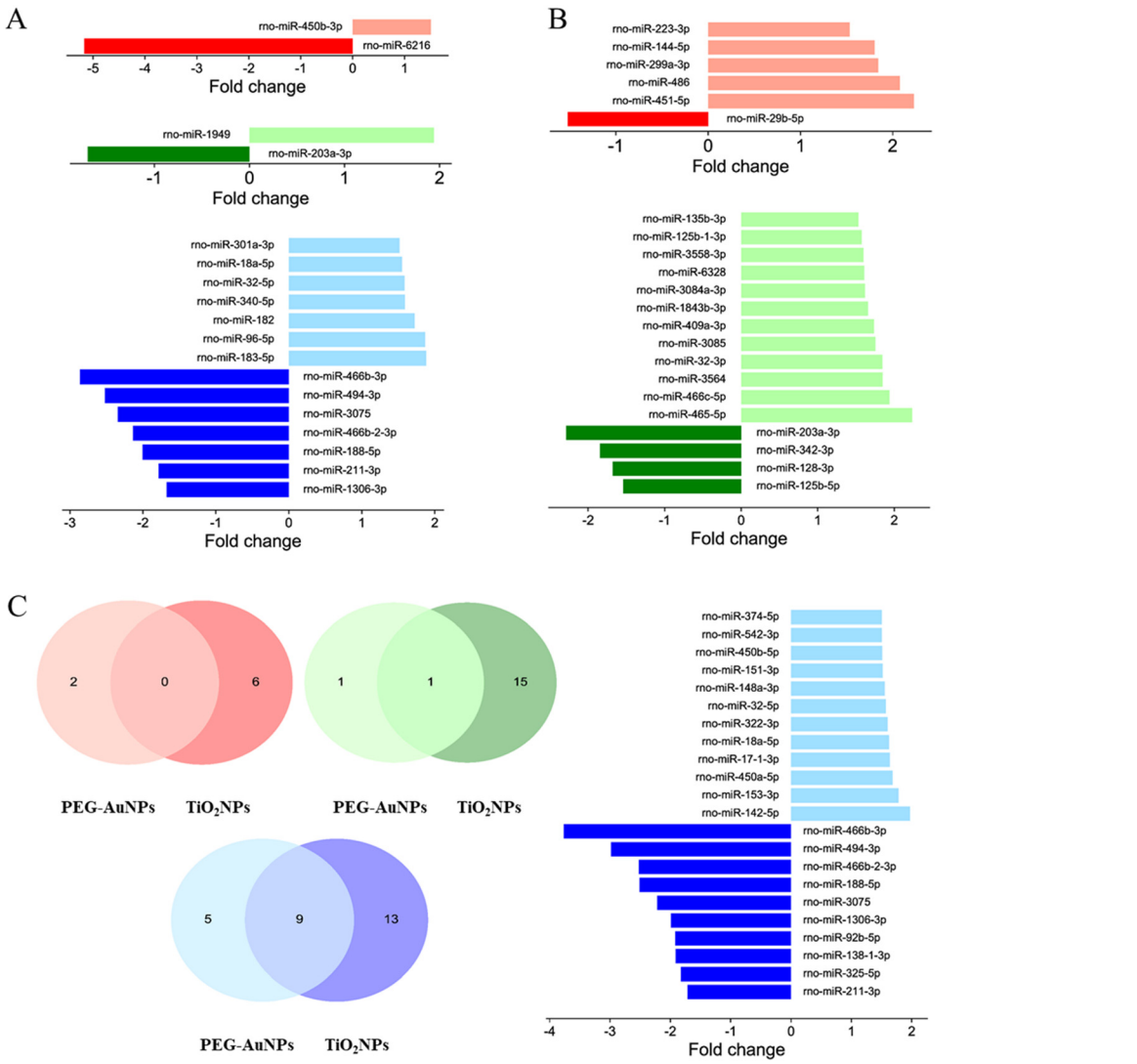

Fig. 4 miRNAs significantly deregulated in the lung (red), liver (green), and kidney (blue) by PEG-AuNPs (A) and TiO_2NPs (B) exposures. Venn diagram showing the overlap between both MNPs-induced miRNA expression changes in individual tissues (C); to distinguish between tissues, see color legend above.

AuNPs; n = 4 – TMAOH, n = 8 TiO_2NPs). Overall, the results acquired by qRT-PCR have been consistent with microarray data (Fig. S3†).

Over-representation pathway analysis using the KEGG database revealed 78 and 47 altered pathways associated with PEG-AuNPs and TiO_2NPs exposure, respectively (Table S8†). Among the ten top-ranked enriched pathways were PPAR signaling, fatty acid metabolism, and degradation. Other significant pathways, mostly related to immune or autoimmune-mediated conditions, were graft-*versus*-host disease, allograft rejection, antigen processing and presentation, autoimmune thyroid disease, type I diabetes mellitus, or insulin signaling pathway. In addition, PEG-AuNP exposure also contributed to deregulating the biosynthesis and metabolism of steroids, carbon, butanoate, terpenoid, and other pathways (Fig. 3A and B). Pathway analysis results for overlapping genes between PEG-AuNPs and TiO_2NPs are shown in Fig. 3C.

MicroRNA expression analysis

Microarray analysis was performed to identify changes in miRNA expression profiles, applying the same cut-off criteria, $p < 0.05$ and FC $\geq$ 1.5, as for mRNA analysis. Unlike changes in mRNA expression, the number of deregulated miRNAs was relatively low (Table 7, Table S9†).

For PEG-AuNPs-treated tissues, only one up- and one down-regulated miRNA were found in the lungs and liver. However, the highest number of candidate miRNAs, seven up-regulated and seven down-regulated, were identified in the kidneys. TiO_2NP exposure induced a more considerable extent of miRNA deregulation, with five up-regulated and one down-regulated miRNA in the lung, 12 down- and four up-regulated miRNAs in the liver, and 10 down- and 12 up-regulated miRNAs in the kidneys. While no miRNA deregulation was observed in the lungs following exposure to studied MNPs, down-regulation of miR-203a-3p, often associated with liver injury, was found in the liver of animals exposed to both PEG-AuNPs and TiO_2NPs. Furthermore, up-regulation of miR-18a-5p and miR-32-5p, previously associated with kidney injury, was identified in both PEG-AuNP and TiO_2NP-exposed kidneys (Fig. 4A and B). However, all 7 down-regulated miRNA detected in the PEG-AuNPs-exposed kidney (rno-miR-466b-3p, rno-miR-494-3p, rno-miR-3075, rno-miR-466b-2-3p, rno-miR-188-5p, rno-miR-211-3p, rno-miR-1306-3p) overlap with findings for TiO_2NPs-exposed tissues, similarly to two up-regulated miRNAs, rno-miR-18a-5p and rno-miR-32-5p (Fig. 4C).

Recently, Falagan-Lotsch & Murphy[68] reported that miRNA expression patterns induced by AuNPs *in vitro* were influenced by treatment conditions (chronic *vs.* non-chronic), surface chemistry, and particles' shape (spherical *vs.* nanorods). Remarkably, non-chronic conditions (24 h exposure to gold nanomaterials followed by cell subcultivation in fresh medium for up to 20 weeks) induced more significant dysregulation in the miRNA levels than the chronic treatment (repeated exposure to gold nanomaterials at 3 day intervals for up to 20 weeks). Under non-chronic treatment conditions, citrate-coated spherical AuNPs induced different miRNA expression patterns than PAA-capped ones. On the other hand, no significant differences in miRNA

Table 8 Integrated prediction of selected deregulated miRNA targets using miRTargetlink 2.0, miRDB, and TargetScan *in silico* tools

Organ	miRNA	MNPs	Genes	Function
Liver	↓rno-miR-203a-3p	PEG-AuNPs	*Aff4*, *Arhgef3*, *Bcl2l11*, *Bicral*, *Ccng2*, *Crebrf*, *Crebzf*, *Dcaf6*, *Ddx3*, *Ebf2*, *Eya4*, *Gabarapl1*, ***Gxylt1***, *Hadhb*, *Hnf4g*, *Ikzf5*, *Ipact*, *Irs2*, ***Itpr2***, *Lats2*, *Mzf1*, *Nfil3*, *Osbpl8*, ***Pptc7***, ***Slc38a2***, *Smim13*, *Tcf7l2*, *Tmx4*, *Tshz3*, *Vegfa*, *Wasf1*, ***Wdfy3***, ***Wsb1***, *Zbtb11*	Tumor suppressor[70]
		TiO_2NPs	*Adamts15*, ***Gxylt1***, *Hrk*, ***Itpr2***, *Nlk*, *Pcmtd1*, *Pim3*, ***Pptc7***, *Ptp4a1*, *Ptpn4*, *Robo2*, *Slc25a21*, ***Slc38a2***, ***Wdfy3***, ***Wsb1***	
Kidneys	↓rno-miR-466b-3p	PEG-AuNPs	Nrg1, Ppm1k, Tmem68	Hypertonic stress-responsive miRNA[71]
		TiO_2NPs	*Arid4a*, *Atp12a*, *Dnajc14*, *Eif1ad*, *Klf11*, *Ndrg4*, *Sbno2*, *Snx19*, *Trib2*, *Wdr44*	
	↓rno-miR-494-3p	PEG-AuNPs	*Hdac8*, *Ms4a6bl*, *Nsg1*	Up-regulation aggravates renal fibrosis and EMT process[76]
		TiO_2NPs	*Cyp26b1*, *Defb29*, *Irs2*, *Snx19*, *Wdr44*	
	↓rno-miR-3075	PEG-AuNPs	*Dmbt1*	Down-regulation associated with partial renal EMT[77]
		TiO_2NPs	—	
	↓rno-miR-466b-2-3p	PEG-AuNPs	*Cyp26a1*, *Nrg1*, *Tmem68*	Hypertonic stress-responsive miRNA[71]
		TiO_2NPs	*Arid4a*, *Eif1ad*, *Fktn*, *Gabbr2*, *Grsf1*, *Ndrg4*, *Rtn1*, *Wdr44*	
	↓rno-miR-188-5p	PEG-AuNPs	—	Down-regulation ameliorates renal EMT[78]
		TiO_2NPs	—	
	↓rno-miR-211-3p	PEG-AuNPs	*Neu3*	Tumor suppressor[72]
		TiO_2NPs	*Ccl21*, *Erbb2*, *Wnt2b*	
	↓rno-miR-1306-3p	PEG-AuNPs	—	Up-regulated in diabetic nephropathy[79]
		TiO_2NPs	—	
	↑rno-miR-18a-5p	PEG-AuNPs	—	Up-regulation associated with kidney injury[74]
		TiO_2NPs	*Trim2*	
	↑rno-miR-32-5p	PEG-AuNPs	—	Up-regulation associated with EMT and renal fibrosis[75]
		TiO_2NPs	*Ddc*, *Insig1*, *Nfyc*, *Per2*, *Pik3cb*, *Usf2*	

Abbreviations: EMT, epithelial to mesenchymal transition.

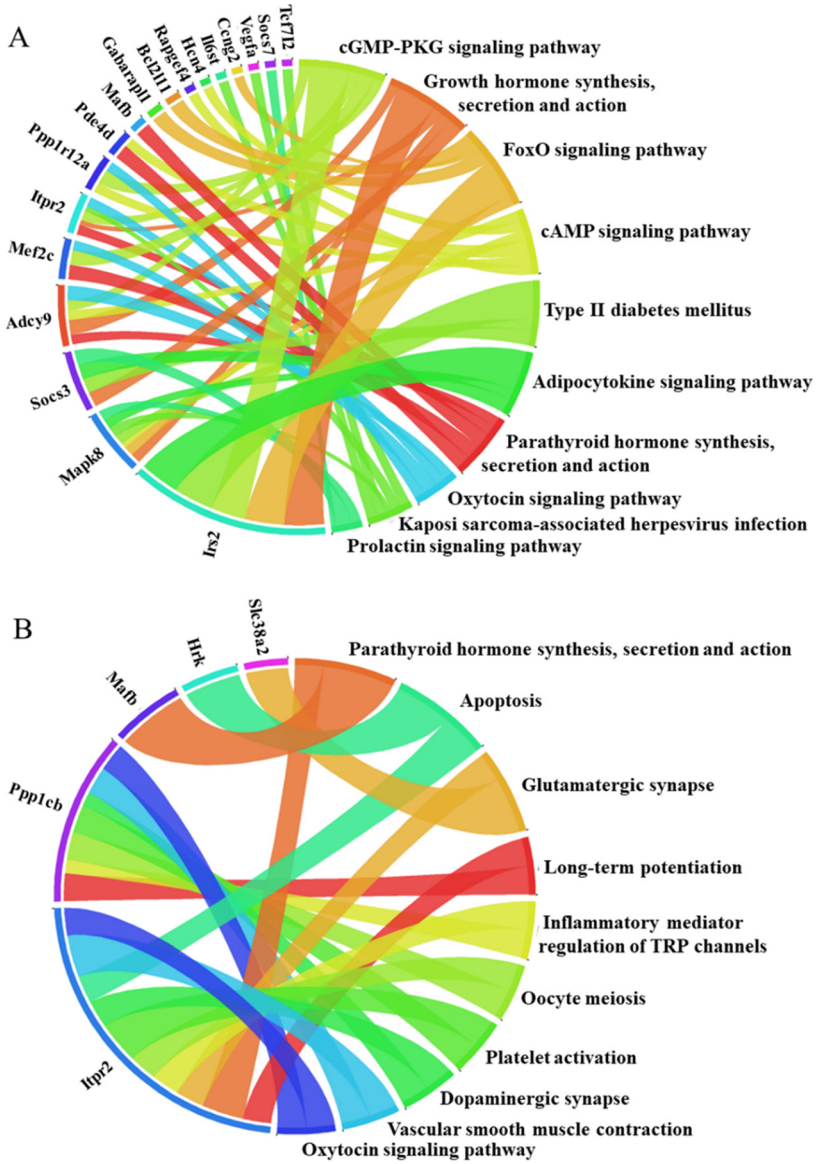

Fig. 5 Results of pathway analysis for nro-miR-203a-3p targets found significantly deregulated by PEG-AuNPs (A) and TiO_2NPs (B). The top ten enriched pathways are presented. The thickness of the lines represents the absolute fold change values of a given gene.

profiles were observed after exposure to Au nanorods (PAA and PEG-coated).

Integrated analysis of miRNA–mRNA expression

To provide more comprehensive information, we conducted the subsequent *in silico* analysis. The data for individual miRNAs were compared with inversely correlated mRNA ($p < 0.05$, FC ≥ 1.5) (Tables 8 and S10†). The potential miRNA–mRNA relationships were predicted using the *in silico* tools miRTargetlink 2.0, miRDB, and TargetScan. The number of predicted targets for individual miRNA ranged from 1 to 93 (Table S9†). Table 8 shows an integrated prediction of overlapped miRNA targets. Only rno-miR-188-5p and rno-miR-1306-3p were not correlated with any target mRNA identified by the microarray gene expression analysis. The largest number of inversely expressed genes were identified for rno-miR-203a-3p.

To further elucidate the potential biological functions and major signaling pathways influenced by deregulated genes included in miRNA–mRNA interactions, we evaluated *in silico* prediction results using pathway analysis tools. This analysis was conducted for rno-miR-203a-3p and its targets, as this specific miRNA was the only one deregulated by both MNP exposures in the liver (Fig. 5). The miR-203 is considered a tumor suppressor. Its down-regulation has been associated with liver fibrosis, EMT promotion, and hepatocellular carcinoma aggressiveness.[69,70] Of note, the down-regulation of nro-miR-203a-3p has inversely correlated with *Slc38A2* and *Wsb1* expression.

In the kidneys, among miRNAs down-regulated by both MNPs were, for example, rno-miR-466b-3p and rno-miR-211-3p.

miR-466a-3p and its close relatives (miR(b/c/e/p)-3p) are important regulators of urine concentration, renal osmoadaptation, and ion homeostasis.[71] Down-regulation of this hypertonic stress-responsive miR-466b-3p might indicate an alteration in renal osmoregulation. Down-regulation of miR-211 promotes histological injury and increases apoptosis in damaged kidneys.[72] Moreover, since miR-211-3p expression in tumor tissue is low, and its up-regulation results in the suppression of cancer cell proliferation, it is considered a tumor suppressor.[73] Remarkably, both MNPs up-regulated rno-miR-18-5p and rno-miR-32-5p in exposed renal tissues. Increased miR-18-5p expression has been associated with kidney injury, EMT, and renal fibrosis.[74,75]

Conclusions

Our study highlights the potential adverse health effects of low-dissoluble NPs, persisting in the tissues due to slow excretion. Observations, such as decreased liver weight and alternations in serum biomarkers, particularly in PEG-AuNPs-exposed rats, suggested disruption in hepatic functions. Persistent residual MNPs deregulated numerous genes in hepatic tissue, with functional classifications in lipid metabolism, cell cycle, and cell proliferation pathways. While PEG-AuNPs and titania NPs induced unique patterns of gene expression change in specific tissues, in the liver, both MNPs deregulated a relatively high number of genes in the same direction associated with liver injury and fibrosis. Additionally, both MNPs down-regulated miR-203a, a tumor suppressor linked to liver fibrosis, EMT promotion, and increased hepatocellular carcinoma aggressiveness. Importantly, integrated miRNA–mRNA analysis revealed several inversely correlated target mRNA identified through microarray gene expression analysis.

Growing evidence shows that deregulation of epigenetic mechanisms is critical in the pathogenesis of various complex human diseases, including cancer.[80] We have shown that chronic exposure to inorganic NPs in human kidney cells caused genome-wide DNA methylome and transcriptome changes.[27] Additionally, significant changes in global DNA methylation were determined in white blood cells from nanomaterial-handling workers[81] and those occupationally exposed to nanocomposite material.[82] Epigenetic alterations might be valuable indicators of adverse health effects of NPs.

An accurate evaluation of the health hazards posed by MNPs, particularly with respect to long-term effects at physiologically relevant concentrations, requires more predictive, sophisticated, and precise approaches. These methodologies should enable a comprehensive multidimensional profiling of complex biological systems. Hence, omics-based risk assessment stands as a crucial tool in identifying novel and more specific nanomaterial-related biomarkers of exposure. Such studies hold significant potential in bridging the gap concerning the safety/hazards of NPs for both human health and the environment. Establishing regulations and guidelines for the production, use, and disposal of NPs, informed by this knowledge, is essential to minimize potential harm effectively.

Author contributions

Andrea Soltysova: investigation (microarray analysis – gene expression), data analysis, curation, and validation, visualization and writing the original initial draft. Nicole Ludwig and Caroline Diener: investigation (microarray analysis – miRNA), data analysis, and curation. Monika Sramkova, Katarina Kozics, Kristina Jakic and Lucia Balintova: investigation, ethical issues management, coordination, and supervision of animal injection with MNPs, tissues/organs sampling for other analyses, data curation. Neus G. Bastus and Oscar Hernando Moriones: investigation (synthesis and characterization of gold and titanium dioxides nanoparticles). Aurelia Liskova and Eva Rollerova: investigation (hematological and immunological analysis). Zora Krivosikova: investigation (Biochemical analysis). Alena Manova and Tibor Dubaj: investigation (quantification of residual MNPs in blood, lungs, liver, kidneys, and spleen). Victor Puntes: supervision MNPs preparation, and characterization. Peter Simon: supervision quantification of MNPs. Ladislava Wsolova: formal analysis – statistical analysis of all data from biological experiments. Jana Tulinska: investigation (immunological analysis – cytokines analysis, data curation, supervision of immunological analysis). Bozena Smolkova: conceptualization, supervision of microarray data (gene expression) analysis, writing the initial original draft. Eckart Meese: supervision of the microarray analysis – miRNA, formal analysis. Alena Gabelova: conceptualization, supervision, and coordination of all experiments and analyses, funding acquisition, visualization, writing the initial original draft. The authors critically reviewed the manuscript, approved the final version, agreed on the journal to which the article has been submitted, and agreed to be accountable for all aspects of the work.

Conflicts of interest

The author reports no conflicts of interest in this work.

Acknowledgements

This paper was supported by the European Union's Horizon 2020 research and innovation program under GA No. 857381 (VISION project) and GA No. 685817 (HISENTS project), DAAD project (Epigenotoxicity of nanomaterials), and APVV 16-0579 (BIONANOGOLD project) and CAS-SAS-2022-14 project.

References

1 S. Bayda, M. Hadla, S. Palazzolo, P. Riello, G. Corona, G. Toffoli and F. Rizzolio, *Curr. Med. Chem.*, 2018, **25**, 4269–4303.
2 S. M. Dadfar, K. Roemhild, N. I. Drude, S. von Stillfried, R. Knüchel, F. Kiessling and T. Lammers, *Adv. Drug Delivery Rev.*, 2019, **138**, 302–325.

3 S. Jafari, B. Mahyad, H. Hashemzadeh, S. Janfaza, T. Gholikhani and L. Tayebi, *Int. J. Nanomed.*, 2020, **15**, 3447–3470.
4 V. Amendola, R. Pilot, M. Frasconi, O. M. Maragò and M. A. Iatì, *J. Phys.: Condens. Matter*, 2017, **29**, 203002.
5 X. Hu, Y. Zhang, T. Ding, J. Liu and H. Zhao, *Front. Bioeng. Biotechnol.*, 2020, **8**, 990.
6 M. Holzinger, A. Le Goff and S. Cosnier, *Front. Chem.*, 2014, **2**, 63.
7 P. Singh, S. Pandit, V. R. S. S. Mokkapati, A. Garg, V. Ravikumar and I. Mijakovic, *Int. J. Mol. Sci.*, 2018, **19**, 1979.
8 D. Ziental, B. Czarczynska-Goslinska, D. T. Mlynarczyk, A. Glowacka-Sobotta, B. Stanisz, T. Goslinski and L. Sobotta, *Nanomaterials*, 2020, **10**, 387.
9 M. Cao, J. Li, J. Tang, C. Chen and Y. Zhao, *Small*, 2016, **12**, 5488.
10 J. Jia, X. Zhou, J. M. Granjeiro, A. Rosa, L. Ribeiro, P. L. Sanches, L. R. De O. Geaquinto, R. Cruz, D. C. Schuck and M. Lorencini, *Front. Bioeng. Biotechnol.*, 2020, **1**, 575.
11 H. Onyeaka, P. Passaretti, T. Miri and Z. T. Al-Sharify, *Curr. Res. Food Sci.*, 2022, **5**, 763–774.
12 H. Ahari, M. Fakhrabadipour, S. Paidari, G. Goksen and B. Xu, *Molecules*, 2022, **27**, 8027.
13 Ş. Sungur, P. Kaya and M. Koroglu, *Food Addit. Contam.: Part B*, 2020, **13**, 260–267.
14 I. Mahapatra, T. Y. Sun, J. R. A. Clark, P. J. Dobson, K. Hungerbuehler, R. Owen, B. Nowack and J. Lead, *J. Nanobiotechnol.*, 2015, **13**, 1–15.
15 E. Baranowska-Wójcik, D. Szwajgier, P. Oleszczuk and A. Winiarska-Mieczan, *Biol. Trace Elem. Res.*, 2020, **193**, 118.
16 R. Mohammadpour, M. A. Dobrovolskaia, D. L. Cheney, K. F. Greish and H. Ghandehari, *Adv. Drug Delivery Rev.*, 2019, **144**, 112–132.
17 M. Bundschuh, J. Filser, S. Lüderwald, M. S. McKee, G. Metreveli, G. E. Schaumann, R. Schulz and S. Wagner, *Environ. Sci. Eur.*, 2018, **30**, 1–17.
18 A. Zielińska, B. Costa, M. V. Ferreira, D. Miguéis, J. M. S. Louros, A. Durazzo, M. Lucarini, P. Eder, M. V. Chaud, M. Morsink, N. Willemen, P. Severino, A. Santini and E. B. Souto, *Int. J. Environ. Res. Public Health*, 2020, **17**, 1–22.
19 P. Nymark, M. Bakker, S. Dekkers, R. Franken, W. Fransman, A. García-Bilbao, D. Greco, M. Gulumian, N. Hadrup, S. Halappanavar, V. Hongisto, K. S. Hougaard, K. A. Jensen, P. Kohonen, A. J. Koivisto, M. Dal Maso, T. Oosterwijk, M. Poikkimäki, I. Rodriguez-Llopis, R. Stierum, J. B. Sørli and R. Grafström, *Small*, 2020, **16**, 1–13.
20 E. Fröhlich, *J. Nanobiotechnol.*, 2017, **15**, 1–22.
21 M. J. B. Amorim, W. Peijnenburg, D. Greco, L. A. Saarimäki, V. I. Dumit, A. Bahl, A. Haase, L. Tran, J. Hackermüller, S. Canzler and J. J. Scott-Fordsmand, *Nano Today*, 2023, **48**, 101735.
22 S. E. Escher, F. Partosch, S. Konzok, P. Jennings, M. Luijten, A. Kienhuis, V. De Leeuw, R. Reuss, K.-M. Lindemann and S. H. Bennekou, *EFSA Supporting Publ.*, 2022, DOI: **10.2903/sp.efsa.2022.EN-7341**.
23 T. H. Shin, S. Nithiyanandam, D. Y. Lee, D. H. Kwon, J. S. Hwang, S. G. Kim, Y. E. Jang, S. Basith, S. Park, J.-S. Mo and G. Lee, *Nanomaterials*, 2021, **11**, 2385.
24 L. Rahman, D. Wu, M. Johnston, A. William and S. Halappanavar, *Mutagenesis*, 2017, **32**, 59–76.
25 M. Husain, D. Wu, A. T. Saber, N. Decan, N. R. Jacobsen, A. Williams, C. L. Yauk, H. Wallin, U. Vogel and S. Halappanavar, *Nanotoxicology*, 2015, **9**, 1013–1022.
26 S. K. Balasubramanian, J. Jittiwat, J. Manikandan, C. N. Ong, L. E. Yu and W. Y. Ong, *Biomaterials*, 2010, **31**, 2034–2042.
27 A. Soltysova, P. Begerova, K. Jakic, K. Kozics, M. Sramkova, E. Meese, B. Smolkova and A. Gabelova, *Cell Biol. Toxicol.*, 2023, **39**, 1939.
28 N. G. Bastus, J. Comenge and V. Puntes, *Langmuir*, 2011, **27**, 11098–11105.
29 T. R. Gordon, M. Cargnello, T. Paik, F. Mangolini, R. T. Weber, P. Fornasiero and C. B. Murray, *J. Am. Chem. Soc.*, 2012, **134**, 6751–6761.
30 K. Kozics, M. Sramkova, K. Kopecka, P. Begerova, A. Manova, Z. Krivosikova, Z. Sevcikova, A. Liskova, E. Rollerova, T. Dubaj, V. Puntes, L. Wsolova, P. Simon, J. Tulinska and A. Gabelova, PEGylated Gold Nanoparticles Vivo, *Nanomaterials*, 2021, **11**, 1702.
31 J. Tulinska, V. Masanova, A. Liskova, M. L. Mikusova, E. Rollerova, Z. Krivosikova, K. Stefikova, I. Uhnakova, M. Ursinyova, J. Babickova, A. Babelova, M. Busova, L. Tothova, L. Wsolova, M. Dusinska, M. Sojka, M. Horvathova, R. Alacova, Z. Vecera, P. Mikuska, P. Coufalik, K. Krumal, L. Capka and B. Docekal, *Food Chem. Toxicol.*, 2020, **136**, 110954.
32 F. Kern, E. Aparicio-Puerta, Y. Li, T. Fehlmann, T. Kehl, V. Wagner, K. Ray, N. Ludwig, H. P. Lenhof, E. Meese and A. Keller, *Nucleic Acids Res.*, 2021, **49**, W409–W416.
33 Y. Chen and X. Wang, *Nucleic Acids Res.*, 2020, **48**, D127–D131.
34 V. Agarwal, G. W. Bell, J. W. Nam and D. P. Bartel, *eLife*, 2015, **4**, e05005.
35 S. Fraga, A. Brandão, M. E. Soares, T. Morais, J. A. Duarte, L. Pereira, L. Soares, C. Neves, E. Pereira, M. de L. Bastos and H. Carmo, *Nanomedicine*, 2014, **10**, 1757–1766.
36 D. Elgrabli, R. Beaudouin, N. Jbilou, M. Floriani, A. Pery, F. Rogerieux and G. Lacroix, *PLoS One*, 2015, **10**, e0124490.
37 M. Mahmoudi, M. P. Landry, A. Moore and R. Coreas, *Nat. Rev. Mater.*, 2023, **8**, 422–438.
38 A. Balfourier, N. Luciani, G. Wang, G. Lelong, O. Ersen, A. Khelfa, D. Alloyeau, F. Gazeau and F. Carn, *Proc. Natl. Acad. Sci. U. S. A.*, 2020, **117**, 103.
39 R. J. B. Peters, A. G. Oomen, G. Van Bemmel, L. Van Vliet, A. K. Undas, S. Munniks, R. L. A. W. Bleys, P. C. Tromp, W. Brand and M. Van Der Lee, *Nanotoxicology*, 2020, **14**, 420.
40 M. Younes, G. Aquilina, L. Castle, K. H. Engel, P. Fowler, M. J. F. Fernandez, P. Fürst, U. Gundert-Remy, R. Gürtler, T. Husøy, M. Manco, W. Mennes, P. Moldeus, S. Passamonti, R. Shah, I. Waalkens-Berendsen, D. Wölfle, E. Corsini, F. Cubadda, D. De Groot, R. FitzGerald, S. Gunnare, A. C. Gutleb, J. Mast, A. Mortensen, A. Oomen, A. Piersma, V. Plichta, B. Ulbrich, H. Van Loveren, D. Benford, M. Bignami,

C. Bolognesi, R. Crebelli, M. Dusinska, F. Marcon, E. Nielsen, J. Schlatter, C. Vleminckx, S. Barmaz, M. Carfí, C. Civitella, A. Giarola, A. M. Rincon, R. Serafimova, C. Smeraldi, J. Tarazona, A. Tard and M. Wright, *EFSA J.*, 2021, **19**, 6585.

41 M. A. K. Abdelhalim and B. M. Jarrar, *Lipids Health Dis.*, 2011, **10**, 1–6.

42 B. Yahyaei, M. Nouri, S. Bakherad, M. Hassani and P. Pourali, *AMB Express*, 2019, **9**, 38.

43 P. C. N. C. Nayak, S. A. Sathar, S. Mughal, S. Duttagupta and M. Mathur, *Virchows Arch.*, 1996, **428**, 353–365.

44 W. S. Cho, M. Cho, J. Jeong, M. Choi, H. Y. Cho, B. S. Han, S. H. Kim, H. O. Kim, Y. T. Lim, B. H. Chung and J. Jeong, *Toxicol. Appl. Pharmacol.*, 2009, **236**, 16–24.

45 M. Botros and K. A. Sikaris, *Clin. Biochem. Rev.*, 2013, **34**, 117–130.

46 P. Steinberg, H. van der Voet, P. W. Goedhart, G. Kleter, E. J. Kok, M. Pla, A. Nadal, D. Zeljenková, R. Aláčová, J. Babincová, E. Rollerová, S. Jaďuďová, A. Kebis, E. Szabova, J. Tulinská, A. Líšková, M. Takácsová, M. L. Mikušová, Z. Krivošíková, A. Spök, M. Racovita, H. de Vriend, R. Alison, C. Alison, W. Baumgärtner, K. Becker, C. Lempp, M. Schmicke, D. Schrenk, A. Pöting, J. Schiemann and R. Wilhelm, *Arch. Toxicol.*, 2019, **93**, 1095–1139.

47 W. Poon, Y. N. Zhang, B. Ouyang, B. R. Kingston, J. L. Y. Wu, S. Wilhelm and W. C. W. Chan, *ACS Nano*, 2019, **13**, 5785–5798.

48 X. Li, B. Wang, S. Zhou, W. Chen, H. Chen, S. Liang, L. Zheng, H. Yu, R. Chu, M. Wang, Z. Chai and W. Feng, *J. Nanobiotechnol.*, 2020, **18**, 1–16.

49 P. Falagan-Lotsch, E. M. Grzincic and C. J. Murphy, *Proc. Natl. Acad. Sci. U. S. A.*, 2016, **113**, 13318–13323.

50 E. M. Grzincic, J. A. Yang, J. Drnevich, P. Falagan-Lotsch and C. J. Murphy, *Nanoscale*, 2015, **7**, 1349–1362.

51 Y. Xiang, Q. Ran, C. Wu, L. Zhou, W. Zhang, J. Li, L. Xiang, Y. Xiao, L. Chen, Y. Chen, X. Chen, A. Stucky, S. C. Li, J. F. Zhong, Z. Li and K. Cai, *Chem. Eng. J.*, 2022, **440**, 135814.

52 L. Rahman, D. Wu, M. Johnston, A. Williams and S. Halappanavar, *Mutagenesis*, 2017, **32**, 59–76.

53 E. Piccinin, M. Cariello, S. De Santis, S. Ducheix, C. Sabbà, J. M. Ntambi and A. Moschetta, *Nutrients*, 2019, **11**, 2283.

54 L. I. Hui, X. Wang, J. Tang, H. Zhao and M. Duan, *Oncol. Lett.*, 2019, **18**, 6214–6220.

55 N. Scaglia, S. Tyekucheva, G. Zadra, C. Photopoulos and M. Loda, *Cell Cycle*, 2014, **13**, 859.

56 J. R. Ow, M. J. Cadez, G. de Zafer, J. C. Foo, H. Y. Li, S. Ghosh, H. Wollmann, A. Cazenave-Gassiot, C. B. Ong, M. R. Wenk, W. Han, H. Choi and P. Kaldis, *eLife*, 2020, **9**, e63835.

57 W. Qian, Z. Zhang, W. Peng, J. Li, Q. Gu, D. Ji, Q. Wang, Y. Zhang, B. Ji, S. Wang, D. Zhang and Y. Sun, *Int. J. Oncol.*, 2018, **53**, 2021–2033.

58 Y. Xiong, L. Ju, L. Yuan, L. Chen, G. Wang, H. Xu, T. Peng, Y. Luo, Y. Xiao and X. Wang, *Oncogene*, 2021, **40**, 1595–1608.

59 H. Yu, H. L. Jiang, D. Xu, J. Z. Jin, Z. M. Zhao, Y. D. Ma and J. Liang, *Cell. Physiol. Biochem.*, 2016, **39**, 700–708.

60 M. Hamada, Y. Tsunakawa, H. Jeon, M. K. Yadav and S. Takahashi, *Exp. Anim.*, 2020, **69**, 1–10.

61 M. Chiba, S. Murata, A. Myronovych, K. Kohno, N. Hiraiwa, M. Nishibori, H. Yasue and N. Ohkohchi, *Int. J. Mol. Med.*, 2011, **27**, 567–574.

62 M. S. Huang, J. H. Chang, W. C. Lin, Y. H. Cheng, F. A. Li, C. S. Suen, M. J. Hwang, C. ke Chang and K. Y. Mou, *Chem. - Asian J.*, 2020, **15**, 3861–3872.

63 H. Xu, H. Han and G. Tian, *J. B.U.ON.*, 2020, **25**, 1890–1896.

64 X. Gao, J. You, Y. Gong, M. Yuan, H. Zhu, L. Fang, H. Zhu, M. Ying, Q. He, B. Yang and J. Cao, *Acta Pharm. Sin. B*, 2022, **12**, 1225–1239.

65 J. He, Y. Li, Y. Wang, H. Zhang, S. Ge and X. Fan, *Oncol. Lett.*, 2018, **15**, 7053–7059.

66 S. Z. Wiley, K. Sriram, C. Salmerón and P. A. Insel, *Int. J. Mol. Sci.*, 2019, **20**, 559.

67 G. Margaillan, M. Rouleau, J. K. Fallon, P. Caron, L. Villeneuve, V. Turcotte, P. C. Smith, M. S. Joy and C. Guillemette, *Drug Metab. Dispos.*, 2015, **43**, 611–619.

68 P. Falagan-Lotsch and C. J. Murphy, *Nanoscale*, 2020, **12**, 21172–21187.

69 Y. Zhao, Z. Wang, J. Zhou, D. Feng, Y. Li, Y. Hu, F. Zhang, Z. Chen, G. Wang, X. Ma, X. Tian and J. Yao, *Toxicol. Appl. Pharmacol.*, 2020, **403**, 115125.

70 M. M. Simile, G. Peitta, M. L. Tomasi, S. Brozzetti, C. F. Feo, A. Porcu, A. Cigliano, D. F. Calvisi, F. Feo and R. M. Pascale, *Oncotarget*, 2019, **10**, 2835–2854.

71 Y. Luo, Y. Liu, M. Liu, J. Wei, Y. Zhang, J. Hou, W. Huang, T. Wang, X. Li, Y. He, F. Ding, L. Yuan, J. Cai, F. Zheng and J. Y. Yang, *Biochim. Biophys. Acta, Gene Regul. Mech.*, 2014, **1839**, 97–106.

72 J. Shang, S. Sun, L. Zhang, F. Hao and D. Zhang, *Bioengineered*, 2020, **11**, 547–557.

73 R. Feng, Z. Li, X. Wang, G. Ge, Y. Jia, D. Wu, Y. Ji and C. Wang, *Cancer Cell Int.*, 2021, **21**, 67.

74 K. L. Connor, O. Teenan, C. Cairns, V. Banwell, R. A. B. Thomas, J. Rodor, S. Finnie, R. Pius, G. M. Tannahill, V. Sahni, C. O. S. Savage, J. Hughes, E. M. Harrison, R. B. Henderson, L. P. Marson, B. R. Conway, S. J. Wigmore and L. Denby, *JCI insight*, 2020, **5**, e140399.

75 H. J. Wang, H. Liu, Y. H. Lin and S. J. Zhang, *Hum. Exp. Toxicol.*, 2021, **40**, 587–595.

76 X. Xue, M. Liu, Y. Wang, Y. Yang, Z. Li, R. Shi and Y. Miao, *Kidney Blood Pressure Res.*, 2022, **47**, 247–255.

77 S. Hajarnis, M. Yheskel, D. Williams, T. Brefort, B. Glaudemans, H. Debaix, M. Baum, O. Devuyst and V. Patel, *J. Am. Soc. Nephrol.*, 2018, **29**, 518–531.

78 M. Xue, Y. Cheng, F. Han, Y. Chang, Y. Yang, X. Li, L. Chen, Y. Lu, B. Sun and L. Chen, *Int. J. Biol. Sci.*, 2018, **14**, 1545–1557.

79 X. Shao, C. Chen, C. Miao, X. Yu, X. Li, J. Geng, D. Fan, X. Lin, Z. Chen and Y. Shi, *Pharmazie*, 2019, **74**, 492–498.

80 V. Buocikova, I. Rios-Mondragon, E. Pilalis, A. Chatziioannou, S. Miklikova, M. Mego, K. Pajuste, M. Rucins, N. El Yamani, E. M. Longhin, A. Sobolev, M. Freixanet, V. Puntes, A. Plotniece, M. Dusinska, M. R.

Cimpan, A. Gabelova and B. Smolkova, *Cancers*, 2020, **12**, 1–32.

81 S. H. Liou, W. Te Wu, H. Y. Liao, C. Y. Chen, C. Y. Tsai, W. T. Jung and H. L. Lee, *J. Hazard. Mater.*, 2017, **331**, 329–335.

82 P. Rossner, K. Vrbova, A. Rossnerova, T. Zavodna, A. Milcova, J. Klema, Z. Vecera, P. Mikuska, P. Coufalik, L. Capka, K. Krumal, B. Docekal, V. Holan, M. Machala and J. Topinka, *Nanomaterials*, 2020, **10**, 550.